Ore Geology Reviews 101 (2018) 870–884

Contents lists available at ScienceDirect

Ore Geology Reviews

journal homepage: www.elsevier.com/locate/oregeorev

Multi-stage Cu remobilization of the Huping metamorphic-hydrothermal deposit in the southern North China Craton

Yan Zhao[a,b,c], Ningbo Li[a,b,*], Yuhang Jiang[a,b], Hecai Niu[a,b], Wubin Yang[a,b]

[a] Key Laboratory of Mineralogy and Metallogeny, Guangzhou Institute of Geochemistry, Chinese Academy of Sciences, Guangzhou 510640, China
[b] Guangdong Provincial Key Laboratory of Mineral Physics and Materials, Guangzhou 510640, China
[c] University of Chinese Academy of Sciences, Beijing 100049, China

ARTICLE INFO

Keywords:
Huping Cu deposit
C–H–O–S isotopes
Fluid inclusion
Metamorphic-hydrothermal remobilization
North China Craton

ABSTRACT

The Zhongtiao region is a well-endowed Cu metallogenic province in the southern North China Craton and contains a large number of early Precambrian Cu deposits of different styles, most of which have been subjected to the ca. 1.85 Ga regional metamorphism. However, whether there was any role for the Proterozoic metamorphism on the extensive Cu mineralization is yet to be well understood. This paper presents an integrated investigation on the field geology, mineral chemistry, fluid inclusion and C–H–O–S isotopes of the Huping metamorphic-hydrothermal deposit in the Neoarchean–Paleoproterozoic Zhongtiao metamorphic terranes, and reveals multi-stage Cu remobilization that formed and upgraded the Cu deposits in the region. We identified three stages of syn- to post-metamorphic Cu remobilization/transportation in the Huping Cu deposit, including (I) early mechanical transport, (II) intermediate metamorphic-hydrothermal remobilization and (III) late meteoric fluid incursion. In stage I, sulfides were remobilized and transported internally under lower-greenschist facies metamorphism, forming the veinlet–disseminated ores and chalcopyrite (avg. $\delta^{34}S$ = 2.1‰, similar to the chlorite-amphibole schist wall rocks). In stage II, the immiscibility of metamorphic fluids (avg. $\delta^{18}O$ = 4.6‰ and δD = −56.6‰) from the metamorphic terranes triggered the precipitation of higher $\delta^{34}S$ chalcopyrite (avg. 8.0‰), led by the incorporation of extra sulfur during the fluid migration. In stage III, incursion of meteoric fluids into the waning metamorphic-hydrothermal system formed the barren quartz-calcite veins (avg. $\delta^{18}O$ = 0.09‰ and $\delta^{13}C$ = −0.88‰). During these Cu remobilization processes, the earlier-formed sulfides were chemically stable during the mechanical transfer by regional metamorphism and deformation. Subsequently, the immiscibility of metamorphic fluids induced significant Cu remobilization and precipitation in the metamorphic-hydrothermal system. We thus propose a model of multi-stage mechanical and chemical Cu remobilization for the Huping Cu deposit, which highlights the crucial impacts of metamorphic-remobilization processes on the regional Cu mineralization in the Zhongtiao region.

1. Introduction

Metamorphic remobilization is a process of micro-, meso-, and macro-scale transformation of preexisting mineralization, resulting in further concentration and redistribution of the ore-forming components (e.g., Marshall and Gilligan, 1987, 1993). Metamorphic remobilization of metals, involving solid-state (mechanical), liquid-state (hydrothermal) or concurrent solid- and liquid-state (mixed) transfer processes (Marshall et al., 2000), has facilitated the formation of metal deposits related to metamorphic events (e.g., Mookherjee, 1970a,b; Tomkins, 2007; Mukwakwami et al., 2014a; Zhang et al., 2014). During regional metamorphism, minerals re-equilibrate to form new assemblages and textures (Pohl, 2011), and the breakdown of volatile-bearing minerals would produce metamorphic fluids (Bickle and Mckenzie, 1987; Connolly and Thompson, 1989; Ferry and Dipple, 1991; Oliver, 1996; Tomkins, 2010). These metamorphic fluids, mixed with other externally-derived fluids (e.g., magmatic fluids from *syn*-metamorphic intrusions or meteoric fluids), may possess mineralization potential (e.g., Stowell et al., 1996; Chen et al., 2004; Mishra and Pal, 2008; Chinnasamy and Mishra, 2013; Mishra et al., 2017). Despite many previous studies on the metamorphic-remobilization processes on hydrothermal deposits in metamorphic terranes (e.g., Stowell et al., 1996; Elmer et al., 2007; Saravanan et al., 2009; Chinnasamy and Mishra, 2013), the detailed metal transfer and precipitation processes are yet to

* Corresponding author at: Key Laboratory of Mineralogy and Metallogeny, Guangzhou Institute of Geochemistry, Chinese Academy of Sciences, Guangzhou 511 Kehua Street, Tianhe District, Guangzhou 510640, China.
E-mail address: liningbo@gig.ac.cn (N. Li).

https://doi.org/10.1016/j.oregeorev.2018.08.030
Received 23 January 2018; Received in revised form 15 August 2018; Accepted 22 August 2018
Available online 23 August 2018

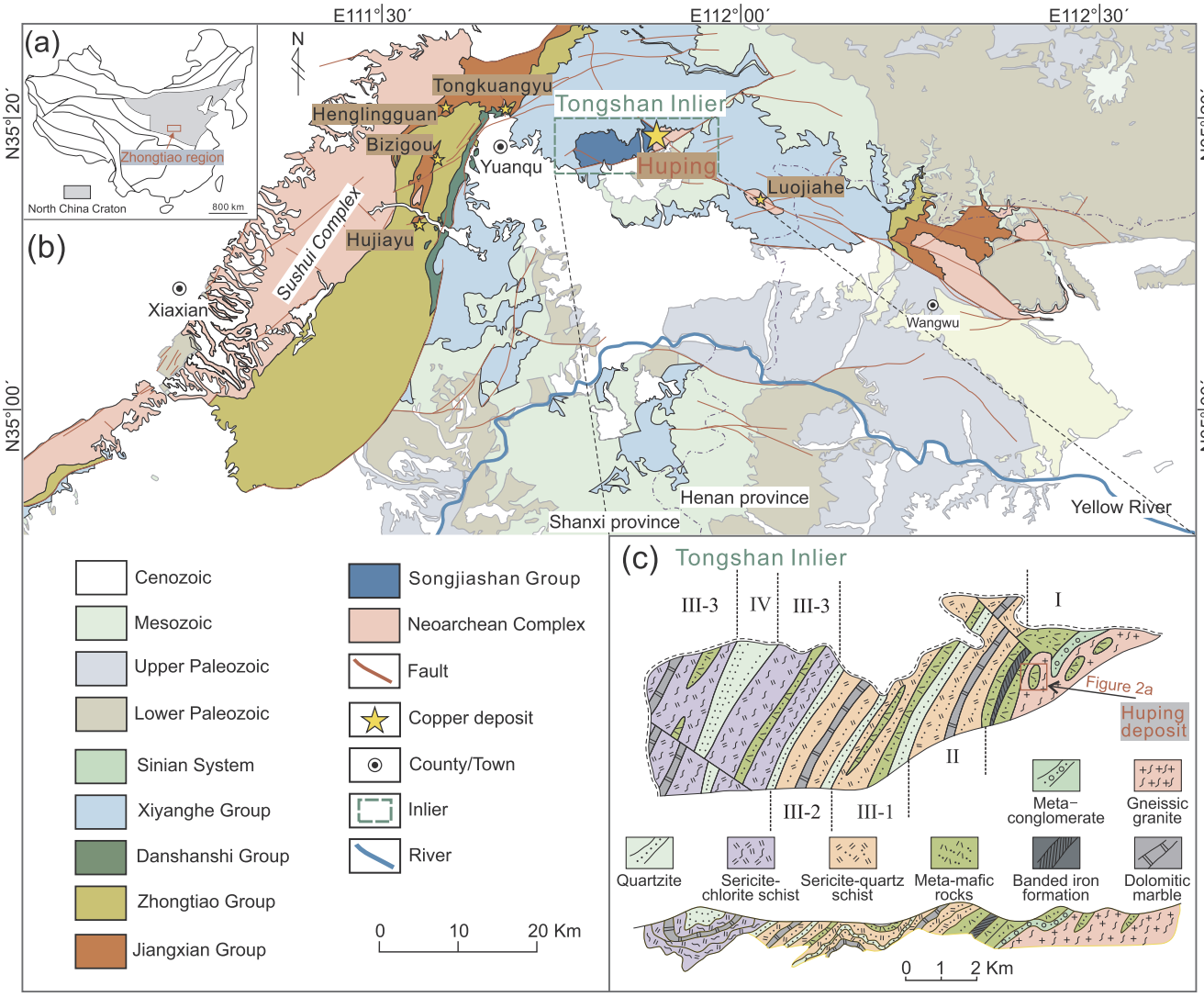

Fig. 1. (a) Regional geologic map of the North China Craton after Zhao and Zhai (2013). (b) Geologic map of the Zhongtiao region, illustrating the distribution of the basement rocks and main Cu deposits (BGMR, 1965; Sun and Hu, 1993). (c) Geologic and profile map of the Tongshan Inlier, showing the lithostratigraphy of the Songjiashan Group and location of the Huping Cu deposit after Sun and Hu (1993); See text for detailed descriptions.

be well understood.

The Zhongtiao region in the southern North China Craton (NCC) is an important Cu metallogenic province in China (Zhai, 2010; Zhai, 2013; Zhai and Santosh, 2013), and hosts over three million tonnes (Mt) of contained Cu (WGCGZM, 1978; Sun et al., 1995). Copper deposits in the Zhongtiao region are mainly hosted in the Neoarchean–Paleoproterozoic metamorphic terranes, and most of these deposits have been subjected to the ca. 1.85 Ga regional metamorphism (Hu and Sun, 1987; Sun et al., 1990; Sun and Hu, 1993). Previous works were mainly focused on determining the original mineralization styles: For example, porphyry Cu affinity has been interpreted for the Tongkuangyu Cu deposit (WGCGZM, 1978; Xu, 2010; Zhang, 2012; Jiang et al., 2014a). The Hujiayu and Bizigou Cu deposits were interpreted to be originally of sediment-hosted (stratiform) type (Zhang, 2012; Jiang et al., 2014b; Qiu et al., 2015a,b), whilst the Luojiahe Cu deposit was interpreted to be a VMS deposit (Jiang et al., 2017). However, the mechanism of Cu mineralization attributed to the later regional metamorphism is still not well understood. Ore deposit geology indicates a hydrothermal Cu deposit affinity for the Huping Cu deposit, which is hosted in the Neoarchean–Paleoproterozoic Zhongtiao metamorphic terranes and shows strong *syn*-metamorphic deformation. This makes the Huping Cu deposit an ideal target to investigate the impact of metamorphic-hydrothermal processes on the original Cu deposit.

In this contribution, integrated investigation on field geology, mineral chemistry, fluid inclusions and C–H–O–S isotopes was conducted, which reveals three stages of syn- to post-metamorphic alteration/mineralization, and a critical Cu upgrading process by the metamorphic-hydrothermal remobilization at Huping. Our study also shed light on the contribution of regional metamorphism to the hydrothermal Cu mineralization.

2. Geologic setting

The NCC is one of the oldest cratons in the world with basement rocks dating back to ~3.8 Ga (Liu et al., 1992; Zhai and Santosh, 2011; Zhao and Zhai, 2013). The Zhongtiao region in the southern NCC contains voluminous outcrops of early Precambrian basement rocks, including those around the Sushui Complex and those within three inliers (i.e., Tongshan, Luojiahe and Wangwu inliers) (Fig. 1a and b). The Precambrian lithologies in the Zhongtiao region include the Late Archean tonalite–trondhjemite–granodiorite (TTG) and supracrustal rocks of the Archean complexes (e.g., the Sushui Complex; Sun and Yu, 1988; Zhang, 2015), the Paleoproterozoic *meta*-volcanic and sedimentary rocks of the Jiangxian Group (ca. 2155 Ma) and the Zhongtiao

Table 1
Comparison of the major Cu deposits in the Zhongtiao region.

Original mineralization		Deposits	Host rocks	Metal	Ore mineral	Dating		
						Sample	Method	Age
Related to volcanism/sub-volcanism	Porphyry mineralization	Tongkuangyu	Quartz-monzonite porphyry; tuff of the upper Jiangxian Group	Major Cu; minor Co, Au, Mo	Py, Ccp, Mo, Co, Bor, Mt	Molybdenite of the Tongkuangyu deposit	Re-Os isochron	2108 ± 38 Ma Chen and Li (1998) 2123 ± 59 Ma (Liu et al., 2016)
	Volcanic-exhalative processes	Huping; Luojiahe	Chlorite schist of the lower Songjiashan Group	Major Cu; minor Co, Au	Ccp, Py, Sp, Bor, Po, Co, Sie	Meta-basic volcanics of the Songjiashan Group	Sm-Nd isochron	~2535 Ma (Sun and Hu, 1993)
Related to sedimentation	Continental environments	Bizigou; Hujiayu	Silicic albitite and dolomitic marble of the lower Zhongtiao Group	Major Cu; minor Co, Au, Ag, Mo	Ccp, Py, Po, Cha, Lin	Intercalated plagioclase amphibolites in the Zhongtiao Group	SIMS zircon U-Pb	2059 ~ 2086 Ma (Liu et al., 2015)
						Uraninite of the Zhongtiao Group	U-Pb concordia	~1832 Ma (Tao, 1985)
	Marine environments	Henglingguan	Sericite mica schist of the lower Jiangxian Group	Major Cu; minor Co, Ni	Ccp, Po,Py, Co	Intercalated plagioclase amphibolites in the Jiangxian Group	SIMS zircon U-Pb	2160–2190 Ma (Liu et al., 2015)
						Monazites from the Cu-bearing veinlets	LA-ICPMS U-Th-Pb	~1863 Ma (Z.J. Qiu et al., 2017)

Abbreviation: Bor–bornite; Cha–chalcocite; Ccp–chalcopyrite; Co–cobaltite; Mo–molybdenite; Mt–magnetite; Po–pyrrhotite; Py–pyrite; Sp–sphalerite; Sie–siegenite; Lin-linneite.

Group (ca. 2104 Ma) (Sun et al., 1992; Liu et al., 2012), the upper Paleoproterozoic thick low-grade *meta*-conglomerate and quartzite of the Danshanshi Group (ca. 1848–1780 Ma) (Liu et al., 2012) and the basaltic to andesitic rocks of the Xiyanghe (or Xionger) Group (ca. 1800–1750 Ma) (Zhao et al., 2007; He et al., 2008). The Songjiashan Group occurs in the western part of the Tongshan Inlier, and consists of four main lithostratigraphic units (Sun and Hu, 1993; Feng and Wang, 2008) (Fig. 1c). The units from the lower to upper part of the Songjiashan Group are as follows: (I) *meta*-mafic volcanics (e.g., chlorite-amphibole schist) with intercalated banded iron formation, which has Sm-Nd isochron age of 2535 Ma (Sun and Hu, 1993) and were intruded by the gneissic granite of ~ 2493 Ma (Zhang, 2012 and our unpublished data), (II) interbedded sericite-quartz schist, dolomitic marble and quartzite, (III) *meta*-sedimentary rocks with minor *meta*-mafic volcanics, and (IV) quartzite. A series of SE-trending and SW-trending basement faults controlled the formation of the Precambrian Cu deposits in the Zhongtiao region, including the Henglingguan, Tongkuangyu, Hujiayu, Bizigou, Luojiahe and Huping deposits (Fig. 1b; Table 1).

Extensive regional metamorphism at ca. 1.85 Ga was documented in the Zhongtiao region and the other parts of the southern NCC (Sun and Hu, 1993; Liu et al., 2006; Wan et al., 2006; Zhao et al., 2008; Trap et al., 2009). Recent U–Th–Pb dating on metamorphic monazites from the Zhongtiao region constrained the timing of peak metamorphism at ca. 1.88 Ga (Qiu et al., 2017a,b). Based on the metamorphic mineral assemblage in the metapelite of the Jiangxian Group, peak metamorphic conditions were approximately estimated at 550–600 °C and 500–700 MPa (Mei, 1994), where over 20 wt% H_2O may have been released by dehydration reactions (Cartwright and Oliver, 2000). Metamorphism resulted in de-hydration reactions of the rocks affected and these might result in the inception of hydrothermal activity in the Zhongtiao region (Hu and Sun, 1987; Sun et al., 1992). Such hydrothermal activities were suspected as the main cause of Cu mineralization in the Zhongtiao region (Sun et al., 1992).

3. Ore deposit geology

The Huping Cu deposit is located in the eastern Tongshan Inlier and hosted in the lower part of the Songjiashan Group (Fig. 1c; 2). The host rocks are mainly chlorite-amphibole schist, which contains high Cu content (over 370 ppm; Han et al., 2005; Wang, 2014) (Fig. 3a). The chlorite-amphibole schist wall rocks contain foliated fine-grained biotite, chlorite and epidote (Fig. 4a), which grow along the crack/cleavage of amphibole (Fig. 4b). Five major tabular or lenticular orebodies, structurally controlled by a series of NW-trending shear zones, have been discovered at Huping (Fig. 2a and b). Such orebodies are imbricated and show an elongation parallel to fold axes or to linear fabrics in surrounding rocks (Fig. 2a and b). Copper mineralization of the Huping Cu deposit is largely stratabound in chlorite-amphibole schist of the Songjiashan Group. Based on mineral assemblages and crosscutting relationships, three stages (I, II and III) of alteration/mineralization have been recognized.

The highly deformed veinlet–disseminated ores were recognized as the stage I mineralization (Fig. 3b). Ore minerals of this stage include chalcopyrite, pyrite and pyrrhotite that occur as thin and discontinuous fabrics parallel to the rock schistosity (Fig. 4c–e). Boudin-like fine-to-medium chalcopyrite aggregates were also observed along the plane of the schistosity (Fig. 4c). Light-green chlorite coexists with chalcopyrite and biotite in the ores of this stage (Fig. 4d).

Thick quartz–sulfide veins (Fig. 3c) were recognized as the stage II mineralization, which contain mainly chalcopyrite, pyrite, pyrrhotite and quartz, and minor bornite (Fig. 4f–h). The ore veins commonly occur along fractures that crosscut the early-stage schistosity (Fig. 3c). Chalcopyrite and gangue minerals in the stage II mineralization are coarse-grained and show no or weak deformation (Fig. 3c).

Comb-textured carbonate (–quartz) veins (Fig. 3d) were recognized

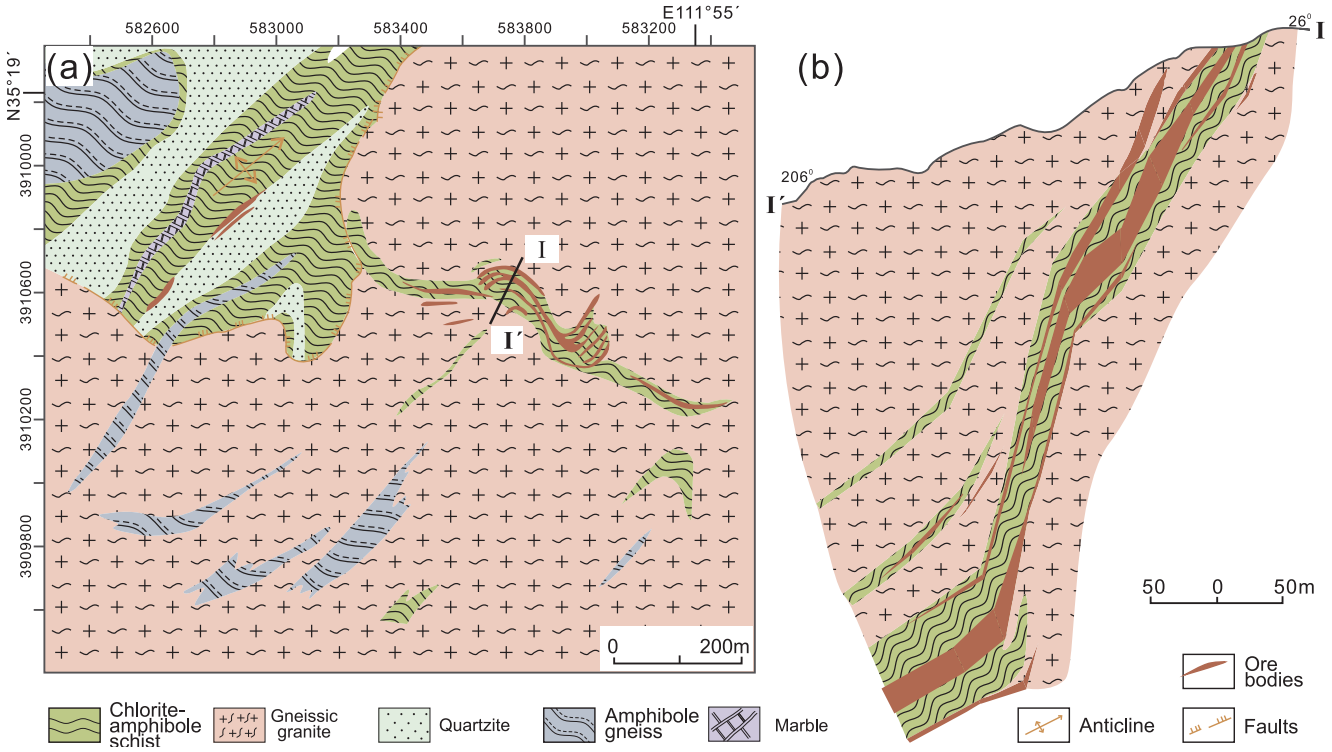

Fig. 2. (a) Geologic map of the Huping Cu deposit and (b) the geologic profile along Exploration Line No. 8, showing the vertical relationships between the orebodies and wall rocks after Sun et al. (1995).

at the stage III alteration. These veins crosscut the stage I and II mineral assemblages (Fig. 4h and i).

The gangue minerals in the Huping Cu deposit include quartz and calcite. Quartz occurs mainly in stage I and stage II but with markedly different occurrence and optical characteristics. Quartz in stage I is strongly deformed and fine-grained, and contains few inclusions (Fig. 4d). In contrast, quartz in stage II is weakly deformed and coarse-grained with numerous fluid inclusions (Fig. 5a–l). Calcite occurs in stage III and contains numerous fluid inclusions (Fig. 5m).

4. Methods

4.1. Major element compositions of chlorite

Major element compositions of eight chlorite samples in stage I ore veins were analyzed at the Key Laboratory of Mineralogy and Metallogeny, Guangzhou Institute of Geochemistry, Chinese Academy of Sciences (GIGCAS) by using a JEOL JXA-8230 electron probe micro-analyzer (EPMA). Operating conditions were 15 kV, 20nA and a 1 μm beam for analyses of all elements. The standards used were BaF_2 for F, tugtupite for Cl, orthoclase for K, albite for Na, kaersutite for Si, diopside for Ca, kaersutite for Al, rhodonite for Mn, rutile for Ti, magnetite for Fe, and olivine for Mg. Raw data were reduced with an online correction procedure including background, dead time and a ZAF calculation. Accuracy and precision are within ~2% relative errors for the major oxides. Parameters of the equipment and procedures are similar to that described by Xing and Wang (2017).

4.2. Fluid inclusion microthermometry and Raman spectroscopy

Twelve quartz and four calcite samples of stage II and III, respectively, were selected for fluid inclusion studies, including petrography, microthermometry and Raman spectroscopy. Microthermometry was conducted at the Key Laboratory of Mineralogy and Metallogeny, GIGCAS by using a Linkam THMS-G-600 heating–freezing stage (−198 to 600 °C). The results were calibrated by using synthetic fluid inclusion standards of pure CO_2 (melting at − 56.6 °C). The precision of temperature measurement is ± 0.1 °C between −100 and 25 °C, ± 1 °C between 25 and 400 °C, and ± 2 °C above 400 °C. The analytical procedures are similar to that described by Jiang et al. (2017).

Laser Raman analyses were conducted at the Key Laboratory of Mineralogy and Metallogeny, GIGCAS, by using the Horiba Xplora Laser Raman Microspectroscopy. An Ar^+ ion laser operating at 44 mW was used to produce an excitation wavelength of 532 nm line. Pure silicon was used as a frequency calibration standard. The scanning range of spectra was set between 1000 and 4000 cm^{-1} with an accumulation time of 20 s for each scan. The spectral resolution was 0.65 cm^{-1}. Details for the operating conditions were described by Jiang et al. (2017).

4.3. In-situ S and mineral C–H–O isotopic analysis

In-situ S isotopic analysis of thirty spots on the stage I and II sulfides were carried out by using Nu Plasma II MC-ICP-MS, which was equipped with the Resonetics-S155 excimer ArF laser ablation system at the State Key Laboratory of Geological Processes and Mineral Resources (GPMR), China University of Geosciences, Wuhan. Helium gas was used to transport the ablated materials into the plasma with a gas flow of 0.35 L/min. Sample gas (argon, 0.65 L/min) was mixed with the carrier gas in a cyclone coaxial mixer before being transported into the ICP torch. The energy fluence of the laser is about 3 J/cm^2. The diameter of laser beam was 33 um with a laser repetition rate of 8 Hz, and the ablation process was set to last for 40 s.

Two in-house pyrite standards (WS-1) were used in this study. The WS-1 (0.9 ± 0.1‰) is a natural pyrite collected from Wenshan polymetallic skarn deposit, Yunnan Province, China. Standard-sample bracketing (SSB) was used to determine the $\delta^{34}S$ values of samples throughout the MC-ICP-MS analytical sessions. The true sulfur isotope ratio was calculated by correction for instrumental mass bias by linear interpolation between the biases calculated from two neighboring

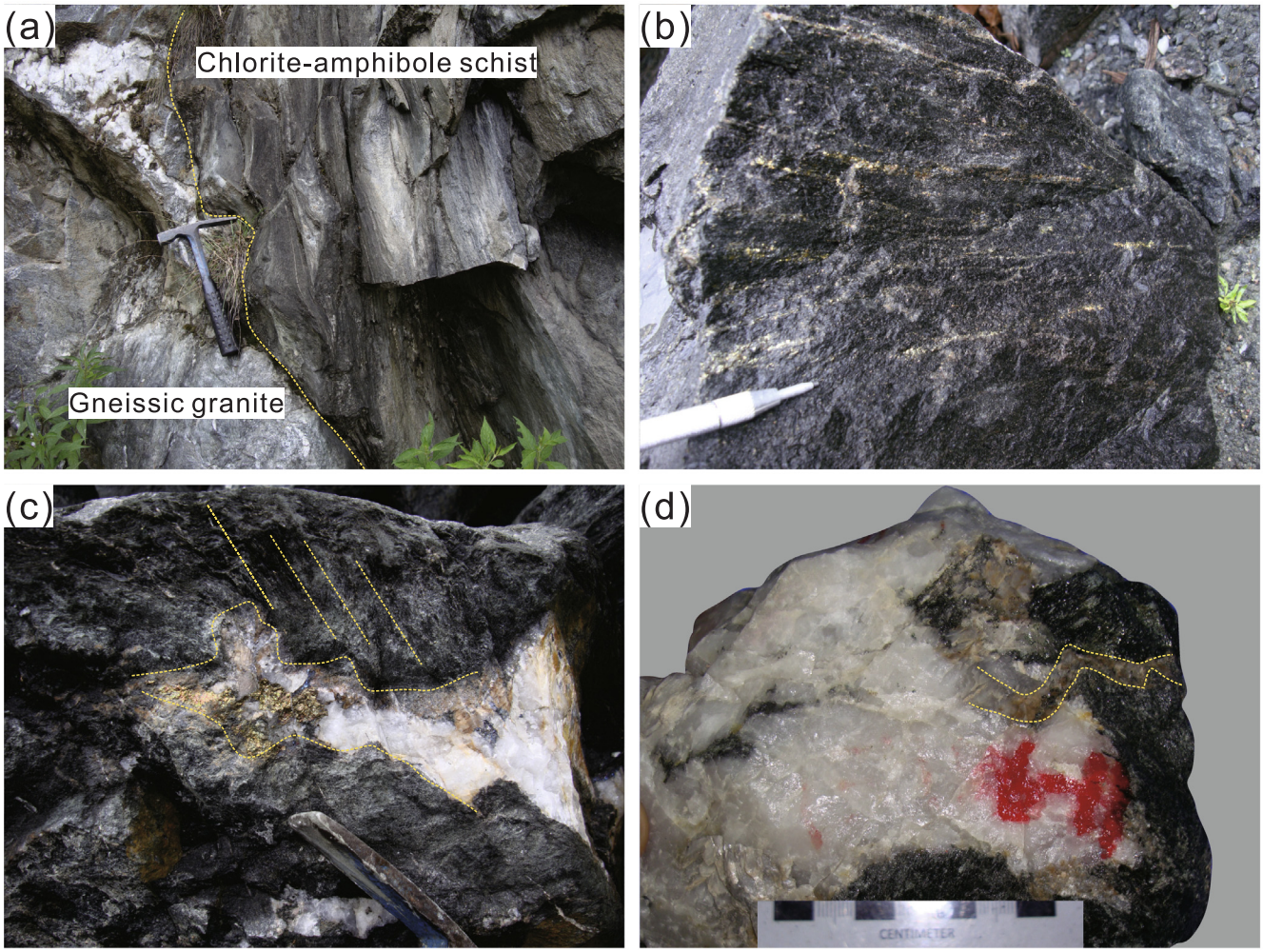

Fig. 3. Photographs showing the ore geology of the Huping Cu deposit. (a) Chlorite-amphibole wall rocks intruded by gneissic granites; (b) Stage I veinlet–disseminated sulfides; (c) Stage II quartz–sulfide veins; (d) Stage III calcite veins.

standard analyses. Isotope ratio data are reported in delta notation (‰) relative to Vienna Cañon Diablo Troilite (V-CDT):

$$\delta^{34}S_{V\text{-}CDT} = [(S/S)_{sample}/(S/S)_{V-CDT} - 1] \times 10^3$$

where $(^{34}S/^{32}S)_{sample}$ is the measured $^{34}S/^{32}S$ ratio of the sample and $(^{34}S/^{32}S)_{V\text{-}CDT}$ is defined as 0.044163 (Ding et al., 2001). The analytical precision (1r) was about ± 0.1 per mil. Detailed analytical conditions and procedures can be seen in Zhu et al. (2016, 2017).

Four quartz samples in stage II ores were selected for H–O isotope analysis and six calcite samples in stage III ores were selected for C–O isotopic analysis. Quartz samples for H–O isotopic analysis were extracted from the crushed rock fragments and handpicked under a binocular microscope. The H–O isotopes were analyzed with a Finnigan MAT253 Mass Spectrometer at the Analytical Laboratory of the Beijing Research Institute of Uranium Geology (BRIUG). All data were normalized to the Vienna standard mean ocean water (V-SMOW) with analytical precisions better than ± 0.2‰ (for $\delta^{18}O$) and ± 1‰ (for δD).

Calcite samples for C–O isotope analysis were powdered to < 200 mesh and were analyzed using a GV Isoprime II Stable Isotope Ratio Mass Spectrometer coupled with an online carbonate preparation system at the State Key Laboratory of Isotope Geochemistry, GIGCAS. Analytical procedures were similar to that described by Deng et al. (2013). $\delta^{13}C$ values were reported as the per mil (‰) deviation of $^{13}C/^{12}C$ relative to the Vienna Pee Dee belemnite (V-PDB) and $\delta^{18}O$ values were reported as the per mil (‰) deviation of $^{18}O/^{16}O$ relative to V-SMOW. External precisions for $\delta^{13}C$ and $\delta^{18}O$ were ± 0.03‰ (1σ) and ± 0.06‰ (1σ), respectively, which were determined by repeated measurements of the international calcite standard NBS-19 and Chinese national standard GBW04405.

5. Results

5.1. Chlorite chemistry and geothermometry

EPMA results (Table 2) show that the chlorites of stage I are ripidolite (Fig. 6). They show narrow compositional ranges of SiO_2 (26.62–27.11 wt%), FeO (18.54–19.40 wt%), MgO (20.04–20.67 wt%) and Al_2O_3 (20.67–21.42 wt%), and are uniformly low in Cr_2O_3, BaO, CaO, K_2O and Na_2O contents.

Crystallization temperatures of the chlorite were calculated using the empirical equation (Cathelineau, 1988):

$$T(C) = -61.92 + 321.98 \times Al(T)$$

where Al (T) represents the tetrahedral Al content. The calculation has the potential to be general applicability for chlorite in diagenetic, hydrothermal and metamorphic settings (Cathelineau, 1988). Calculated temperatures of the stage I chlorite vary in a narrow range of 332–349 °C (avg. 344 °C; Table 2).

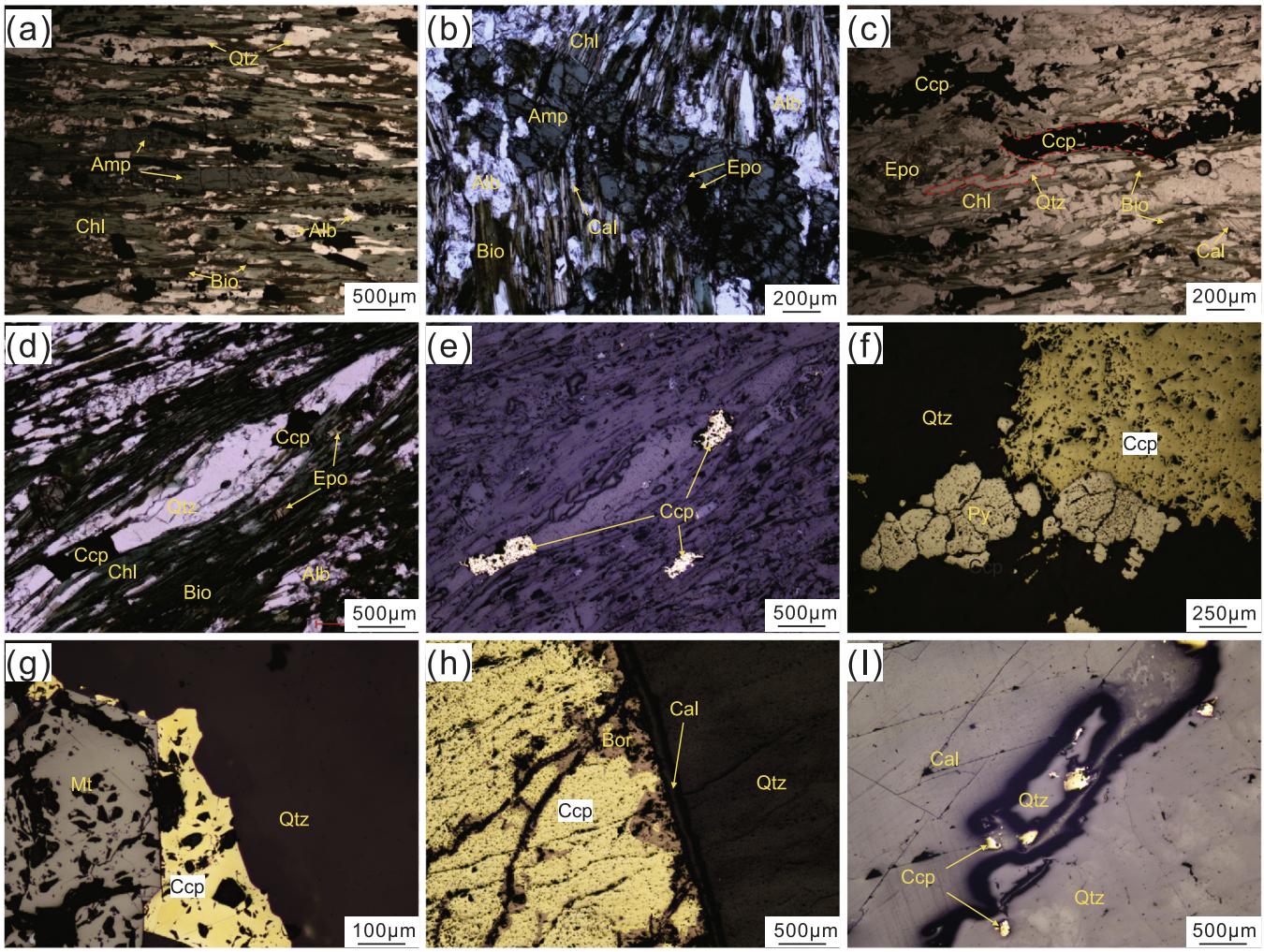

Fig. 4. Photomicrographs of the Huping Cu deposit. (a, b) Mineral assemblages of the wall rock chlorite-amphibole schist; (c) Elongated boudin-like chalcopyrite aggregates; (d, e) Stage I chalcopyrite and gangue minerals; (f–h) Mineral assemblage and textures for the stage II mineralization; (i) Stage III calcite crosscutting stage II quartz and sulfides. *Abbreviations*: Alb–Albite; Amp–Amphibole; Bio–Biotite; Bor–Bornite; Cal–Calcite; Ccp–Chalcopyrite; Chl–Chlorite; Epo–Epidote; Mt–Magnetite; Py–Pyrite; Qtz–Quartz.

5.2. Fluid inclusion results

5.2.1. Fluid inclusion petrography

At room temperature, three types of fluid inclusion were observed in quartz and calcite: vapor-rich two- or three-phase CO_2-bearing (type I), daughter mineral bearing (type II) and liquid-rich two-phase (type III) fluid inclusions.

Type I inclusions contain two or three phases ($L_{H2O} + L_{CO2} \pm V_{CO2}$) at room temperature and have various CO_2 phase volumetric proportions (generally $V_{CO2} > 40$ vol%). They show negative crystal, rounded or elliptic shapes with size of ~6 to 16 μm (Fig. 5c–g), and are isolated or randomly distributed. Type I inclusions generally occur in clusters with type II inclusions in stage II quartz (Fig. 5a–d).

Type II inclusions contain daughter minerals and are rich in liquid ($L_{H2O} + D + V_{H2O}$). They range in size of ~8 to 20 μm and typically show rounded or negative crystal shapes (Fig. 5h–l). Daughter minerals of the type II inclusions mainly include halite and sylvite with possible captive hematite and opaque minerals. The opaque minerals are brassy and irregularly shaped under reflected light (Fig. 5k and l), resembling chalcopyrite. Type II and type I inclusions are the major fluid inclusion types in stage II quartz, which commonly occur in the core of quartz, and are thus probably primary (Fig. 5a and b).

Type III inclusions consist of a vapor bubble and a liquid phase ($L_{H2O} + V_{H2O}$) at room temperature. They are rounded or rectangular shaped and range in size of ~ 4 to 15 μm (Fig. 5m). The vapor phase of the inclusions normally occupies 5 to 15 vol%. Type III inclusions are the main fluid inclusion type in stage III calcite and commonly occur along calcite cleavage (Fig. 5m).

5.2.2. Fluid inclusion microthermometry and Raman spectroscopy

The microthermometric results are listed in Table 3 and illustrated in Fig. 7. For type I inclusions ($L_{H2O} + L_{CO2} + V_{CO2}$), calculations for salinity (wt% NaCl eqv) were made by melting temperature of CO_2 clathrates, based on equation of Diamond (1992). Molar volume (cc/mol) was estimated by V–X diagram of the H_2O–CO_2 fluid system (Bakker and Diamond, 2000), using the homogenization temperatures and modes of the carbonic phase (Th_{CO2}), and estimation of the volumetric proportion of the carbonic at Th_{CO2}. Then the software LonerAP (Bakker, 2012) was used to calculate isochores. For halite-bearing type II inclusions (L_{H2O} + Halite + V_{H2O}), dissolution temperature of halite (Tm_{hal}) was used to determine salinity based on equation of Hall et al. (1988). For type III inclusions ($L_{H2O} + V_{H2O}$), salinities were calculated by measuring the freezing point of the solution (Tm_{ice}) as described by Bodnar (1993), and isochores were determined using the software SOWAT (Driesner, 2007).

For type I inclusions in stage II quartz, the melting of the carbonic phase (Tm_{CO2}) occurred between −57.4 and −56.2 °C, suggesting the

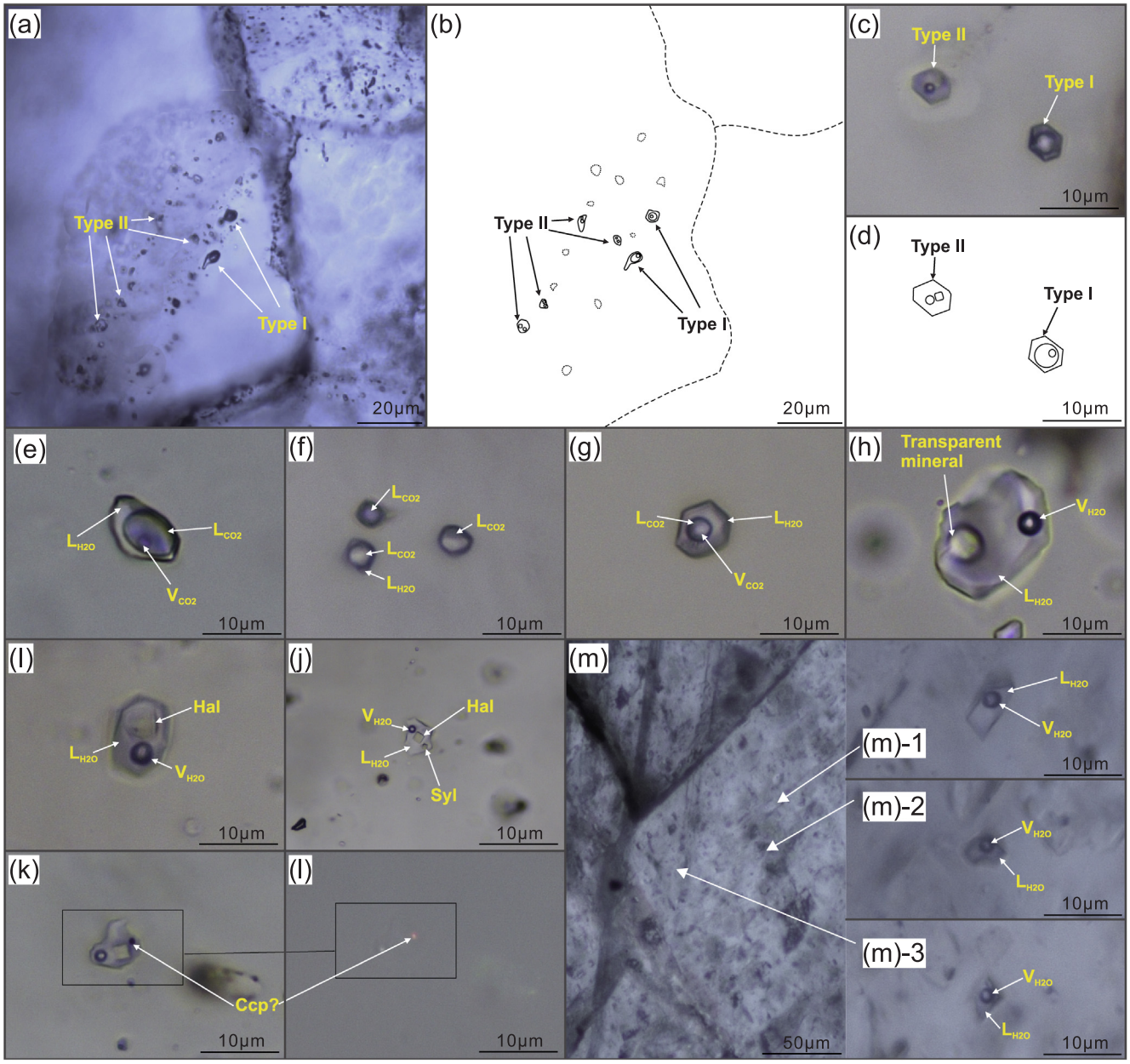

Fig. 5. Photomicrographs showing petrographic characteristics of fluid inclusions from the Huping Cu deposit. (a, b) Photomicrograph and corresponding sketch map, showing the distributions of type I and II inclusions in the stage II mineralization; (c, d) Photomicrograph and corresponding sketch map, showing the negative-crystal type I and II inclusions; (e–g) Representative type I inclusions (L_{H2O} + L_{CO2} ± V_{CO2}); (h–j) Representative type II inclusions (L_{H2O} + D + V_{H2O}); (k, l) Opaque mineral-bearing type II inclusions under transmitted and reflected light, respectively; (m, m_{1-3}) Type III inclusions in stage III primary calcite. *Abbreviations*: V_{CO2}–CO_2 vapor; L_{CO2}–CO_2 liquid; V_{H2O}–H_2O vapor; L_{H2O}–H_2O liquid; Ccp–Chalcopyrite; Hal–Halite; Syl–Sylvie.

phase is nearly pure CO_2. The final clathrate melting (Tm_{cla}) occurred between 4.0 and 9.7 °C, corresponding to salinities between 8 and 13 wt % NaCl eqv. Homogenization of the carbonic phase in type I inclusions (Th_{CO2}; L_{H2O} + L_{CO2} + V_{CO2} → L_{H2O} + L_{CO2}) occurred by vapor bubble disappearance between 2.7 and 29.0 °C. Total homogenization (Th_{total}; L_{H2O} + L_{CO2} → L) occurred mainly at 300–380 °C (minor at 400–440 °C).

For type II inclusions (halite as daughter mineral) in stage II quartz, vapor bubble disappearance (Th_{bubble}; L_{H2O} + halite + V_{H2O} → L_{H2O} + halite) occurred at 110–299 °C. Th_{total} (L_{H2O} + Halite → L) fell between 280 and 360 °C, corresponding to salinities of 34–38 wt% NaCl eqv.

For type III inclusions in stage III calcite, ice-melting temperatures (Tm_{ice}) ranged from − 17.8 to − 1.4 °C, corresponding to salinities of 2.4–20.8 wt% NaCl eqv. Th_{total} (L_{H2O} + V_{H2O} → L) fell between 153 and 229 °C.

The Raman spectroscopy results (Fig. 8) of representative inclusions show that the vapor phase of type I inclusions is composed of CO_2, and the aqueous phase is mainly composed of H_2O (Fig. 8a and b). Aqueous and vapor phases of type II and III inclusions are also composed of H_2O (Fig. 8c–f).

5.3. *In-situ* S and mineral C–H–O isotopic compositions

In-situ S isotopic results are listed in Table 4 and illustrated in Fig. 9. The stage I chalcopyrite has $\delta^{34}S$ values varying from 1.7‰ to 2.5‰ (avg. 2.1‰), whereas the stage II chalcopyrite and pyrite have $\delta^{34}S$ values varying from 7.4‰ to 8.8‰ (avg. 8.0‰) and 9.2‰ to 10.2‰

Table 2
EPMA results of chlorite, along with their structural formulae and calculated temperatures.

	15HP6 − 1–2				15HP6 − 1–19			
	01	02	03	04	01	02	03	04
SiO_2	26.74	26.74	27.11	26.62	26.89	26.62	27.05	26.87
Al_2O_3	20.91	21.22	20.73	21.20	20.98	20.98	20.67	20.79
FeO	19.16	18.54	18.74	18.59	19.05	18.71	18.66	19.40
MnO	0.21	0.25	0.24	0.22	0.19	0.22	0.21	0.22
MgO	20.33	20.45	20.04	20.33	20.32	20.11	20.67	20.22
Total	87.35	87.20	86.87	86.95	87.42	86.63	87.26	87.50
Cations								
Si	2.73	2.73	2.78	2.72	2.74	2.74	2.76	2.75
Al	2.51	2.55	2.50	2.55	2.52	2.54	2.48	2.50
Fe	1.64	1.58	1.60	1.59	1.62	1.61	1.59	1.65
Mn	0.02	0.02	0.02	0.02	0.02	0.02	0.02	0.02
Mg	3.09	3.11	3.06	3.10	3.09	3.08	3.14	3.08
Structural formula								
Si (T)	2.73	2.73	2.78	2.72	2.74	2.74	2.76	2.75
Al (T)	1.27	1.27	1.22	1.28	1.26	1.26	1.24	1.25
(T) total	4.00	4.00	4.00	4.00	4.00	4.00	4.00	4.00
Al (O)	1.25	1.27	1.27	1.28	1.26	1.27	1.24	1.24
Mg (O)	3.09	3.11	3.06	3.10	3.09	3.08	3.14	3.08
Fe (O)	1.64	1.58	1.60	1.59	1.62	1.61	1.59	1.65
Mn (O)	0.02	0.02	0.02	0.02	0.02	0.02	0.02	0.02
(O) total	5.99	5.98	5.95	5.98	5.99	5.97	5.99	5.99
T/°C	346	348	332	349	343	345	338	342

Note: (T): Cations in tetrahedral sites; (O): Cations in octahedral sites; T: Temperature calculated using empirical calibrations of Cathelineau (1988).

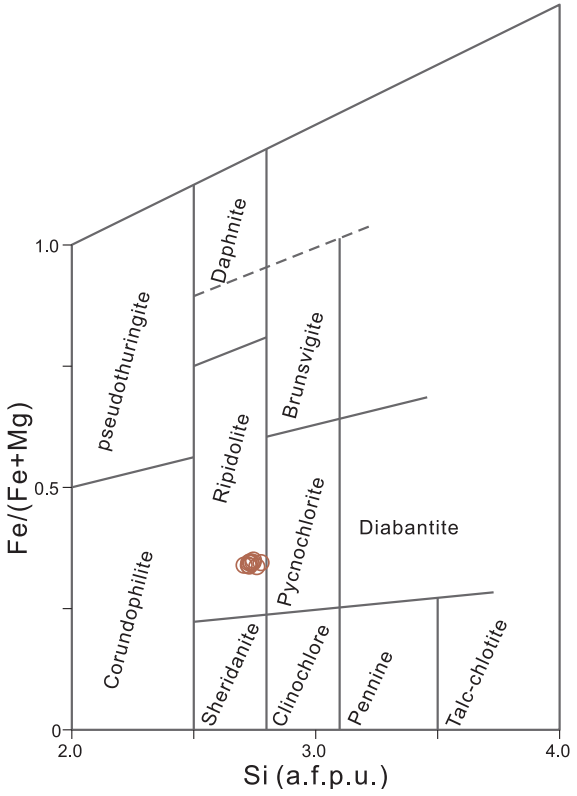

Fig. 6. Fe/(Fe + Mg) vs. Si (a.f.p.u., atoms per formula unit) diagram of the Huping chlorite. Nomenclature and boundaries are after Hey (1954).

(avg. 9.8‰), respectively. The $\delta^{34}S$ values of the equilibrium fluids were calculated from the sulfide $\delta^{34}S$ and the mineral–H_2S fractionation factor of Ohmoto and Goldhaber (1997), assuming H_2S as the major sulfur species in the fluids. The calculated $\delta^{34}S_{H2S}$ values of the stage I chalcopyrite vary in the ranges of 1.8 to 2.7‰ (avg. 2.2‰), using the chlorite thermometric results. The calculated $\delta^{34}S_{H2S}$ values of the stage II chalcopyrite and pyrite vary in the ranges of 7.6 to 9.0‰ (avg. 8.2‰) and 8.0 to 9.2‰ (avg. 8.7‰), respectively, using the fluid inclusion microthermometric results.

Mineral C–H–O isotopic results are listed in Table 5 and illustrated in Figs. 10 and 11. $\delta^{18}O$ values of the stage II quartz fall in a narrow range of 10.7‰ to 11.9‰ (avg. 11.5‰). The calculated $\delta^{18}O$ values of the equilibrium fluids vary from 3.8‰ to 5.0‰ (avg. 4.6‰), using the equation ($1000\ln\alpha_{quartz\text{-}water} = 3.38 \times 10^6 T^{-2} - 3.40$) of Clayton et al. (1972) and the average Th_{total} of fluid inclusions in quartz (~320 °C). In addition, the δD values of the extracted fluids from the stage II quartz vary from −63.9‰ to − 49.3‰ (avg. −56.6‰). The $\delta^{13}C$ values of the stage III calcite vary from − 1.26 to −0.71‰ (avg. −0.88‰) relative to PDB, and the $\delta^{18}O$ values vary from 10.57 to 11.62‰ (avg. 10.92‰) relative to V-SMOW. $\delta^{18}O$ values of the equilibrium fluids in stage III were calculated at − 0.27 to 0.78‰ (avg. 0.09‰), using the calcite–H_2O equilibrium equations (O'Neil et al., 1969; Faure, 1986) and the average Th_{total} of fluid inclusions in calcite.

6. Discussion

6.1. Three stages of Cu mineralization

Deformation of the orebodies and intense hydrothermal alteration at Huping suggest that the original mineralization had been modified by later remobilization processes. The original Huping Cu mineralization was proposed to be attributed to the eruption of the Songjiashan Group mafic volcanic rocks (Sun et al., 1995; Wang, 2014), resembling VMS type, as evidenced by the high Cu content (over 370 ppm) of the Songjiashan Group (Han et al., 2005; Wang, 2014) and the largely stratabound nature of the Cu orebodies. As to be described below, the geologic and isotopic characteristics revealed in this study reflect a complex metamorphic Cu remobilization history that had formed and upgraded many of the Huping Cu orebodies. The remobilization processes include deformation and metamorphism (stage I), metamorphic-hydrothermal alteration (stage II), and meteoric fluid incursion (stage III).

6.1.1. Stage I: Mechanical transfer

The ore geologic and isotopic characteristics indicate that the stage I mineralization was triggered by mechanical remobilization, which was interpreted to represent solid-state ductile transfer including plastic and cataclastic flow and entrainment (Marshall and Gilligan, 1987). Firstly, the veinlet–disseminated ores and the absence of fluid inclusions in quartz (Fig. 4d) suggest weak fluid activities during the stage I mineralization. Secondly, chlorite in this stage occurs as ripidolite (Fig. 6), which is generally related to metamorphism (Wang et al., 1982). The metamorphism had likely thickened and upgraded the orebodies at the fold hinges (Sun et al., 1995; Wang, 2014). Last but not least, chalcopyrite in stage I has relatively low $\delta^{34}S$ values (avg. 2.1‰), resembling those of the Songjiashan Group wall rocks (Fig. 9).

6.1.2. Stage II: Metamorphic-hydrothermal remobilization

The presence of fissure-controlled/-filling veined ores in the stage II mineralization indicates hydrothermal remobilization, which was interpreted to represent liquid-state transport by solution diffusion (Marshall and Gilligan, 1987). Compared to those of stage I, $\delta^{34}S$ values of sulfides in stage II are more positive (Fig. 9). The calculated $\delta^{34}S$ values (7.6‰ to 9.1‰) of the stage II equilibrium fluids are higher than those of the majority of magmatic-hydrothermal deposits (−3 to 1‰; Hoefs, 2009), but overlap with the metamorphic fluid-related orogenic-type deposits (0 to 10‰; Goldfarb and Groves, 2015) (Fig. 9). In addition, δD (−63.9‰ to − 49.3‰) and the calculated $\delta^{18}O$ (3.8‰ to 5.0‰) values of the stage II fluids fall into the overlapping area of metamorphic and magmatic fluids (Taylor, 1974) (Fig. 10). These H–O

Table 3
Microthermometric data of the type I, II and III inclusions for the Huping deposit.

Type	Num.	Size/μm	Vapor/CO_2 proportion	Tm_{CO2}/°C	Tm_{ice}/°C	Tm_{cla}/°C	Th_{CO2} /°C	Th_{bubble}/°C	Th_{total}/Tm_{hal}/°C	Salinity/wt% NaCl eqv
I	25	10 to 20	20 to 40%	−57.4 to −56.2 (avg. −57.0)		−2.0 to 6.1 (avg. 3.7)	2.7 to 29.0 (avg. 19.2)		302 to 435 (avg. 363)	7.3 to 17.4 (avg. 10.7)
II	40	5 to 25	~5%					110 to 209 (avg. 170)	205 to 406 (avg. 291)	31.6 to 37.0 (avg. 34.5)
III	19	4 to 20	Mostly 5 to 10%		−16.7 to −8.5 (avg. −8.8)				153 to 229 (avg. 178)	12.3 to 20.0 (avg. 15.4)

Abbreviations: Tm_{CO2} = Final melting temperature of the carbonic phase, Tm_{ice} = Final ice melting temperature, Tm_{cla} = Final clathrate melting temperature Th_{CO2} = Homogenization temperature of the carbonic phase, Th_{bubble} = Vapor bubble disappearance temperature, Th_{total} = Temperature of final homogenization, Tm_{hal} = Final halite melting temperature.

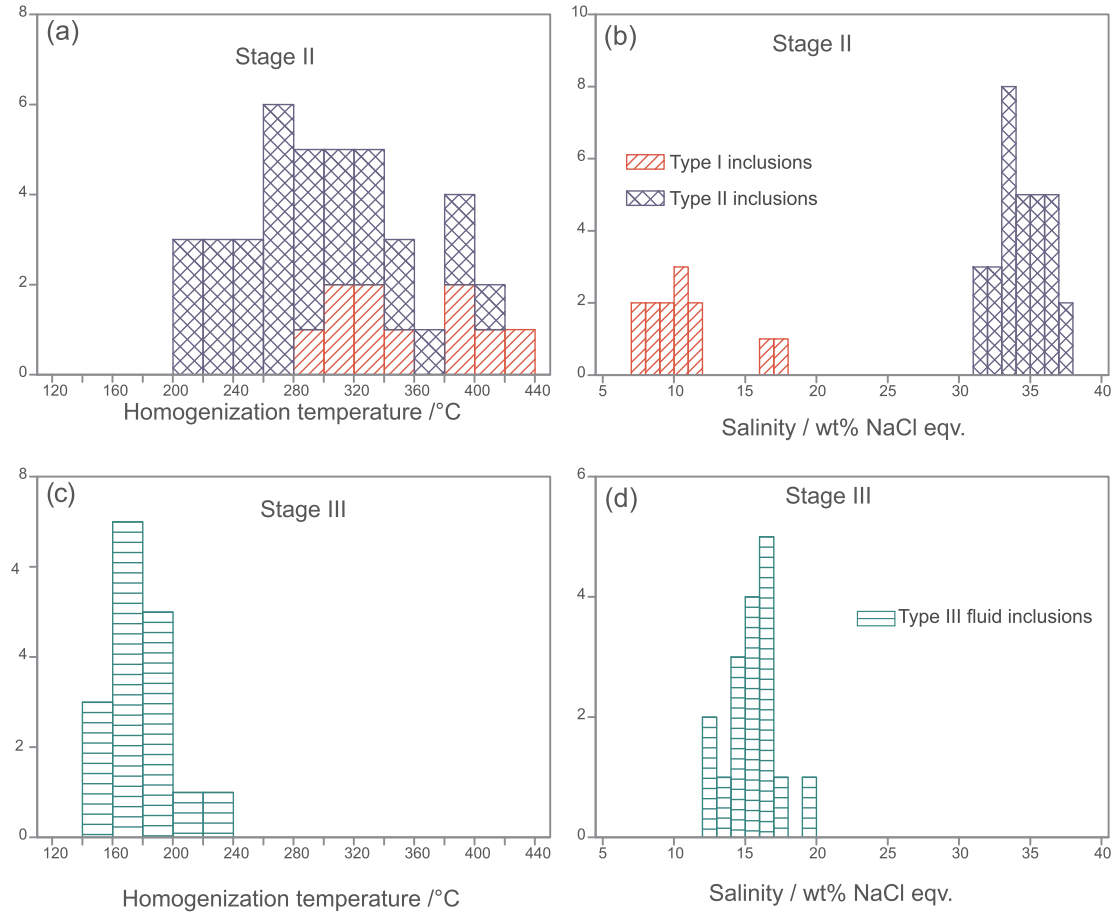

Fig. 7. Histograms of (a) homogenization temperatures and (b) salinities for fluid inclusions in stage II quartz. Histograms of (c) homogenization temperatures and (d) salinities for fluid inclusions in stage III calcite.

isotopic compositions are also similar to the fluids of the metamorphic-hydrothermal stages of the Hujiayu and Bizigou Cu deposits in the Zhongtiao region (Hu and Sun, 1987; Sun et al., 1995; Jiang et al., 2014b) (Fig. 10). Thus, we infer that the stage II ore-forming fluids were likely metamorphic-sourced.

Ore precipitation from the metal-bearing fluids is controlled by various physicochemical factors (Hemley et al., 1992; Robb, 2013), including temperature and/or pressure drop (e.g., Landtwing et al., 2005; Wang et al., 2013), fluid immiscibility (boiling/effervescence) (e.g., Klemm et al., 2007; Chen et al., 2012; Zhao et al., 2013; Qiu et al., 2017a,b), fluid mixing (e.g., Chi and Savard, 1997; Chen et al., 2004; Qiu et al., 2016a), and fluid–rock interactions (e.g., Williams-Jones et al., 2010; Peng et al., 2016). At Huping, the narrow H–O isotope range (Fig. 10) does not support the presence of significant fluid mixing or fluid-rock interactions. In contrast, the fault-controlled orebodies and the open-fracture filling features of the ores indicate that pressure drop may have facilitated the ore precipitation. Pressure drop would generally lead to the migration of H_2O–CO_2 solvus to higher temperatures, causing fluid immiscibility (Brown, 1998). The separation of a homogeneous aqueous-carbonic fluid into an aqueous and a CO_2-rich fluid likely happened in the stage II mineralization. This is supported by (1) the coexistence of the type I and II inclusions (Fig. 5a–d) with similar homogenization temperatures but different homogenized nature and distinct salinities (Fig. 7; Table 3) in stage II quartz, and (2) the presence of rare carbonic inclusions with almost no aqueous phase (Fig. 5f). This phase separation process is consistent with what would be expected during fluid immiscibility (Ramboz et al., 1982). Immiscibility of CO_2-bearing fluids would promote the precipitation of both gangue and ore minerals (Robb, 2013). Therefore, fluid immiscibility induced by decompression may have been the main trigger

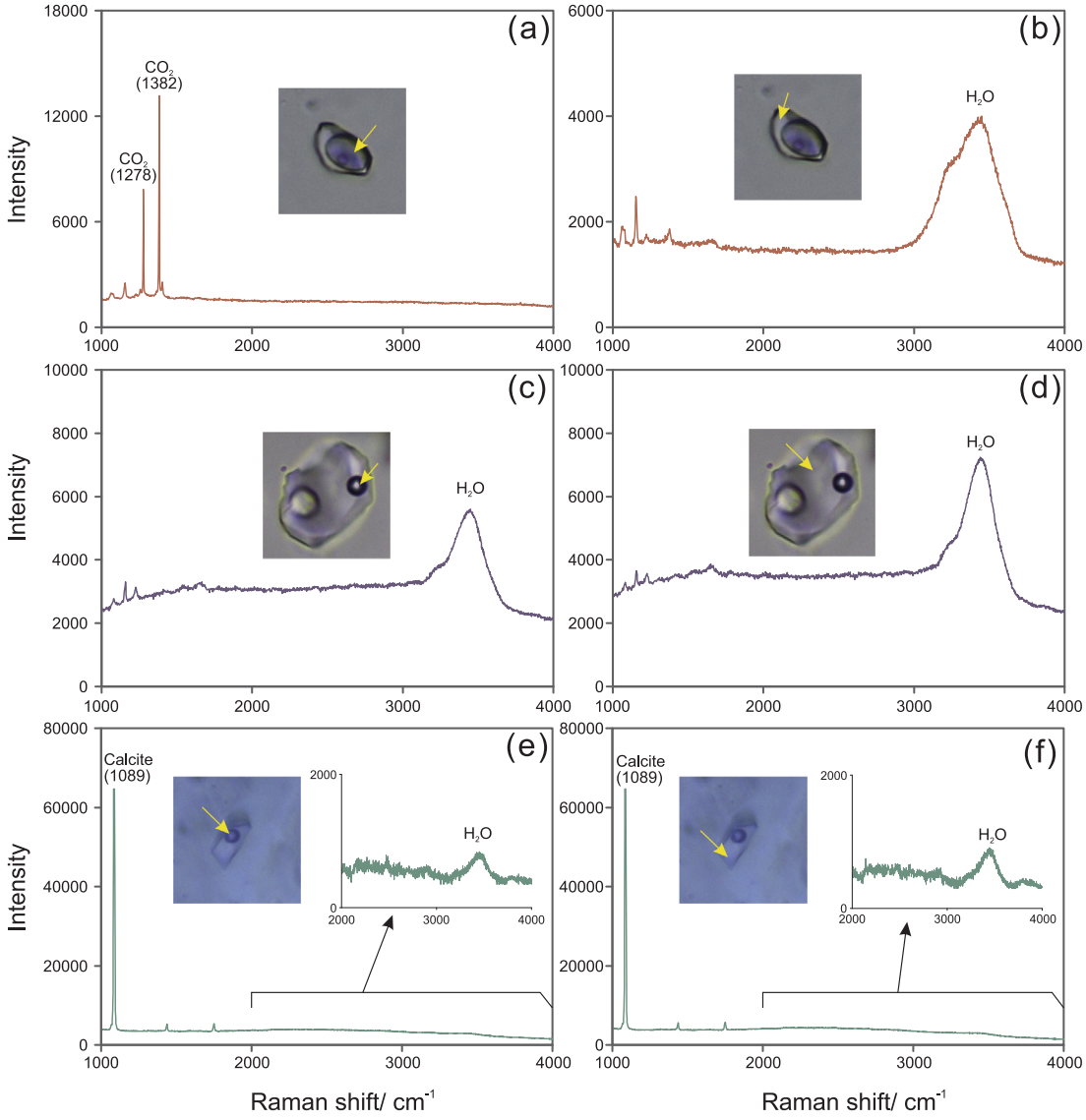

Fig. 8. Raman spectra of representative fluid inclusions. (a) Carbonic and (b) liquid phase in type I inclusions; (c) Vapor and (d) liquid phase in type II inclusions; (e) Vapor and (f) liquid phase in type III inclusions.

Table 4
Sulfur isotopic compositions of sulfides in the Huping deposit.

Sample	Mineral	$\delta^{34}S$/‰	Stage	Sample	Mineral	$\delta^{34}S$/‰	Stage
15HP6-1–1-01	Ccp	1.8	I	15HP19-1–05	Ccp	8.3	II
15HP6-1–1-02	Ccp	1.9	I	15HP19-1–06	Ccp	8.8	II
15HP6-1–1-03	Ccp	2.1	I	15HP6-18–2-01	Ccp	7.7	II
15HP6-1–1-04	Ccp	2.0	I	15HP6-18–2-02	Ccp	7.4	II
15HP6-1–1-05	Ccp	2.0	I	15HP6-18–2-04	Ccp	7.7	II
15HP6-1–1-06	Ccp	1.7	I	15HP6-18–2-05	Ccp	8.3	II
15HP6-1–2-01	Ccp	2.4	I	15HP6-18–2-08	Ccp	7.7	II
15HP6-1–2-02	Ccp	2.2	I	15HP6-18–2-10	Ccp	7.9	II
15HP6-1–2-03	Ccp	2.4	I		$\delta^{34}S_{H2S}$	7.6–9.0	
15HP6-1–2-04	Ccp	2.3	I				
15HP6-1–2-05	Ccp	2.5	I	15HP6-18–2-03	Py	9.4	II
15HP6-1–2-06	Ccp	2.1	I	15HP6-18–2-06	Py	10.1	II
	$\delta^{34}S_{H2S}$	1.8–2.7		15HP6-18–2-07	Py	10.2	II
				15HP6-18–2-09	Py	10.0	II
15HP19-1–01	Ccp	8.0	II	15HP6-18–2-11	Py	9.8	II
15HP19-1–02	Ccp	7.6	II	15HP6-18–2-12	Py	9.2	II
15HP19-1–03	Ccp	8.3	II		$\delta^{34}S_{H2S}$	8.0–9.2	
15HP19-1–04	Ccp	8.6	II				

Abbreviations: Ccp–Chalcopyrite, Py–Pyrite. $\delta^{34}S_{H2S}$ values are calculated for pyrite–H_2S and chalcopyrite–H_2S equilibrium. See text for discussion.

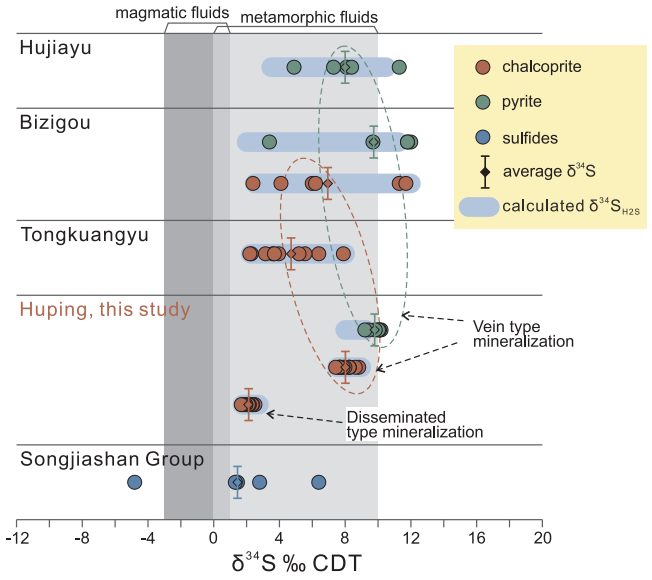

Fig. 9. Sulfide $\delta^{34}S$ and calculated $\delta^{34}S_{H2S}$ values of the stage I and II mineralization of the Huping Cu deposit. $\delta^{34}S_{H2S}$ values are calculated based on pyrite–H_2S and chalcopyrite–H_2S equilibrium. See text for discussion. Sulfur isotope and mineralization temperature data of the Tongkuangyu, Bizigou, Hujiayu and Luojiahe deposits and the wall rock Songjiashan Group are from Sun et al. (1995), Jiang et al. (2014a; 2014b) and Zhang (2012). Sulfur isotopic data of magmatic and metamorphic fluids are from Hoefs (2009) and Goldfarb and Groves (2015), respectively.

Table 5
Carbon, hydrogen and oxygen isotopic results of the Huping deposit.

Sample	Mineral	Stage	$\delta^{13}C$ /‰ V-PDB (mineral)	$\delta^{18}O$ /‰ V-SMOW (mineral)	δD /‰ V-SMOW (fluids)	$\delta^{18}O$ /‰ V-SMOW (fluids)
14HPK1-5	Qtz	II		11.6	−54.3	4.7
14HPK1-9	Qtz	II		11.9	−58.8	5.0
14HPK1-3	Qtz	II		11.8	−63.9	4.9
14HPK1-6	Qtz	II		10.7	−49.3	3.8
14HPK1-9-1	Cal	III	−0.74	10.57		−0.27
14HPK1-9-2	Cal	III	−0.80	10.58		−0.26
15HP6-19	Cal	III	−0.87	10.60		−0.23
15HPK1-6	Cal	III	−0.87	11.42		0.59
14HPK1-2	Cal	III	−0.71	10.73		−0.10
14HPK1-9	Cal	III	−1.26	11.62		0.78

Abbreviations: Qtz–Quartz, Cal–Calcite.

for the stage II Cu precipitation at Huping.

6.1.3. Stage III: Meteoric fluid incursion

Carbon and oxygen isotopes suggest that incursion of meteoric fluids into the metamorphic-fluid-dominated hydrothermal system may have happened during stage III. $\delta^{18}O$ values of equilibrium fluids decrease from stage II to stage III (Fig. 11a), suggesting a low $\delta^{18}O$ source for the latter, e.g., meteoric fluids. $\delta^{13}C$ values of the stage III calcite are higher than those of average organic matter, atmospheric CO_2, dissolved CO_2 in fresh water, continental crust, igneous rocks/magmatic systems and mantle, but lower than those of average marine carbonates (Fig. 11b). This suggests that the CO_2 in the stage III fluids was likely sourced from a mixture of marine carbonates (possibly the Songjiashan Group dolomitic marble; Fig. 1c) and a low $\delta^{13}C$ source, e.g., meteoric fluids with atmospheric CO_2 (Fig. 11b).

6.2. P–T conditions of mineralization

Mineralization related to metamorphic fluids is hosted in a variety

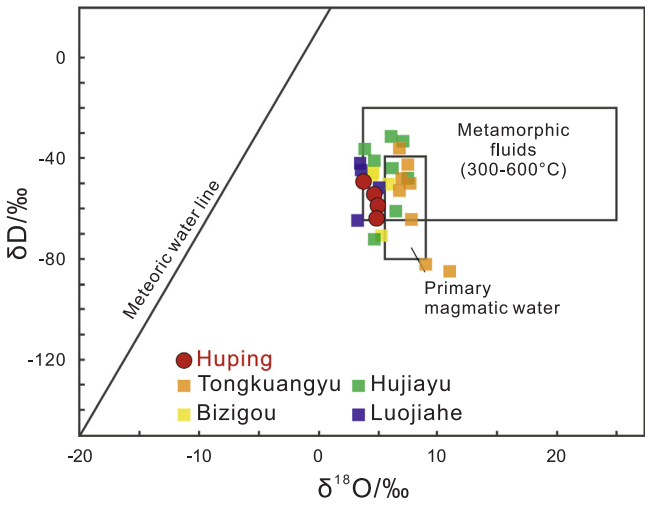

Fig. 10. Calculated H–O isotopic compositions of equilibrium fluids in the stage II mineralization of the Huping Cu deposit. H–O isotope data of metamorphic-hydrothermal veins of the Tongkuangyu, Bizigou, Hujiayu and Luojiahe deposits were compiled from Jiang et al. (2016; 2017) and Sun et al. (1995).

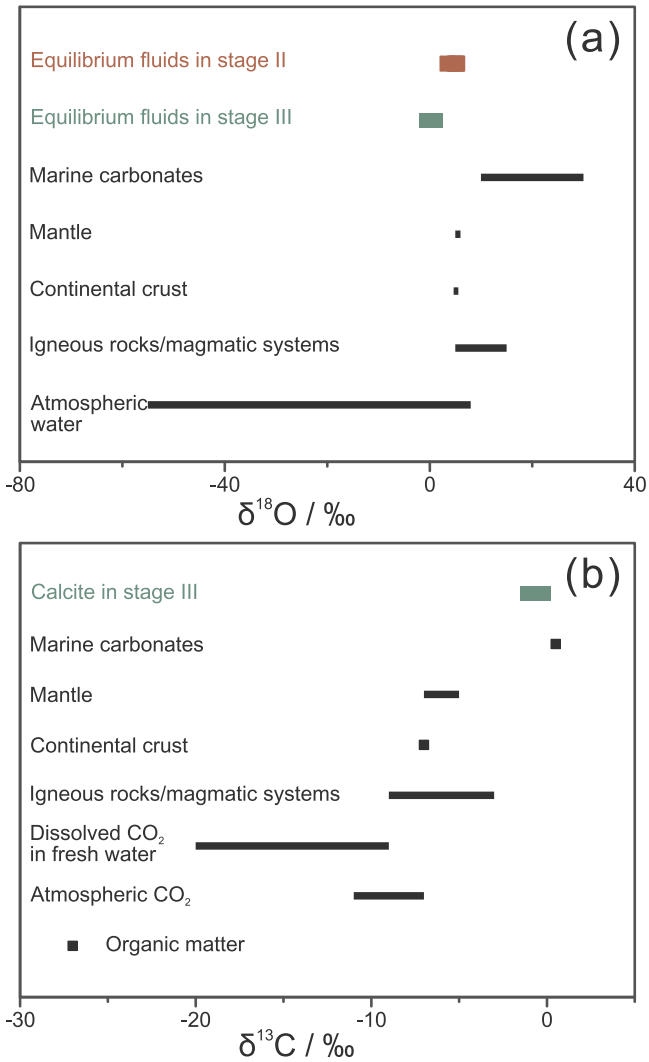

Fig. 11. (a) Calculated $\delta^{18}O$ values of equilibrium fluids and (b) $\delta^{13}C$ values of calcite in stage III of the Huping Cu deposit. References for major carbon and oxygen reservoirs are from Hoefs (2009).

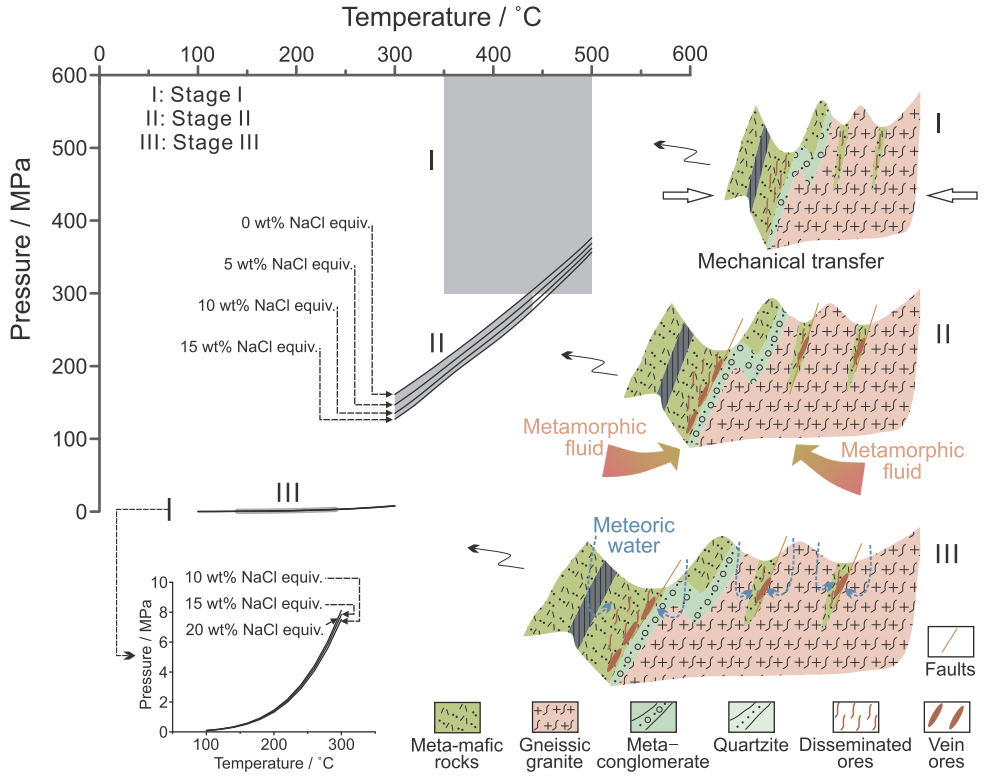

Fig. 12. P–T conditions and schematic sketches illustrating the three stages of ore mineralization in the Huping Cu deposit.

of lithologies, which were metamorphosed to greenschist facies, and less commonly to lower amphibolite facies (Pirajno, 1992). Previous studies show that the depositional conditions of metamorphic fluids are characterized by a temperature range of approximately 200 to 450 °C (mainly 250 to 350 °C), at pressures of 0.5 to 4 kbar (Pirajno, 1992). Therefore, P–T conditions could be critical to metamorphic-hydrothermal mineralization.

Stage I of the Huping Cu deposit has a gangue mineral assemblage of albite + chlorite + biotite + epidote (Fig. 4d), indicative of lower greenschist facies metamorphic conditions (ca. 350–500 °C and 300–800 MPa; Spear, 1995). The metamorphic temperature is consistent with our estimated chlorite formation temperature (332–349 °C). The trapping temperature and pressure of fluid inclusions likely recorded the P–T conditions of the hydrothermal system (Ramboz et al., 1982; Brown, 1998). Giving that fluid immiscibility had likely occurred during the stage II mineralization, the overlapping peak temperatures (300–360 °C) for type I and II inclusions can be considered as the temperature of the stage II ore-forming fluids. The corresponding trapping pressures were estimated to be around 120 to 300 MPa, based on a series of H_2O–NaCl–CO_2 isochores with different salinities. Besides, low temperature and pressure conditions (< 250 °C and < 10 MPa) for stage III is constrained by the microthermometric results of type III inclusions in calcite, i.e., the 150–230 °C homogenization temperatures and isochores of H_2O–NaCl system with different salinities. Therefore, we conclude that the stage I mineralization of the Huping Cu deposit likely occurred under lower greenschist facies metamorphic conditions; the stage II mineralization may have occurred at post-peak metamorphic ca. 300–360 °C and 120–300 MPa conditions, which is consistent with the main P–T range of ore deposition from metamorphic fluids; the stage III alteration may have occurred under low P–T conditions (Fig. 12).

P–T conditions of the Huping Cu deposit indicate that the main Cu deposition occurred during the post-peak metamorphism, yielding the fissure-controlled/-filling veined ores, which is consistent with the occurrence of Cu-mineralization in metamorphic rocks worldwide (Pirajno, 1992). Fluid decompression has been recognized as a highly efficient mechanism for the characteristic co-precipitation of silica with metals during vein formation (Weatherley and Henley, 2013). As discussed above, decompression is critical to fluid immiscibility and thus the Cu mineralization at Huping.

6.3. Mechanisms of Cu remobilization

Mechanical and hydrothermal remobilization in the sulfide ore formation in metamorphic terranes have been supported by many research (Mishra et al., 2005; Tomkins, 2007; Mukwakwami et al., 2014a,b; Zhang et al., 2014; Turlin et al., 2016; Qiu et al., 2017a,b). Previous studies show that mechanical remobilization is ineffective in remobilizing disseminated sulfides for any significant distance (Tomkins, 2007). The minor Cu endowment in the veinlet–disseminated ores of the Huping Cu deposit also indicates that Cu was unlikely to be significantly mobilized by the stage I mechanical transfer.

Metamorphic-hydrothermal remobilization has been proposed to be a critical process for Cu mineralization (e.g., Turlin et al., 2016; Qiu et al., 2017a,b), which can enrich Cu by dissolution and subsequent reprecipitation of sulfides during or after peak metamorphism (Mukwakwami et al., 2014a,b). The increase of sulfide $\delta^{34}S$ from the mechanical transfer (stage I) to metamorphic-hydrothermal alteration (stage II) indicates the incorporation of extra sulfur during the migration of metamorphic fluids, which could increase the stability of Cu hydrosulfide/sulfide complexes in aqueous hydrosulfide solutions (Mountain and Seward, 2003; Qiu et al., 2015a,b, 2016b) and thus Cu solubility in the mineralizing fluids. Most Cu would precipitate by the cooling of Cu-saturated fluids from 350 to 250 °C (Xiao et al., 1998), which is consistent with our fluid inclusion results. The main Cu endowment in the vein-type ores at Huping, and the occurrence of stage II metamorphic-fluid immiscibility indicate that Cu mineralization was mainly achieved by the immiscibility of Cu-bearing metamorphic fluids.

Most Cu deposits in the Zhongtiao region (Fig. 1b) were subjected to the metamorphism, independent of their various original

mineralization styles (Hu and Sun, 1987; Sun and Hu, 1993; Sun et al., 1995). For example, late-stage, metamorphic-remobilization-related thick quartz–calcite veins were recognized at the Tongkuangyu, Bizigou, Hujiayu and Luojiahe deposits (e.g., Hu and Sun, 1987; Sun and Hu, 1993; Sun et al., 1995; Jiang et al., 2014a,b; Qiu et al., 2015a,b; Jiang et al., 2017). In addition, ore remobilization during the post-orogenic exhumation (which upgrades the Cu ore veinlets and lenses) has recently been documented at the Henglingguan deposit (Qiu et al., 2017a,b). Hydrothermal remobilization of these Cu deposits was generally interpreted to be related to the ca. 1.85 Ga regional metamorphism (e.g., Zhang, 2012; Jiang et al., 2014b, 2017; Liu et al., 2016; Qiu et al., 2015a,b,2017a,b). The Huping Cu deposit has metamorphic-hydrothermal-related ore features, mineral assemblages and fluid H–O and sulfide S isotopic compositions (Figs. 9 and 10) similar to many other Cu deposits in the region. Therefore, the metamorphic-hydrothermal remobilization of the Huping Cu deposit was likely attributed to the ca. 1.85 Ga regional metamorphism. The syn- to post-peak metamorphic Cu transfer and remobilization processes at Huping indicate crucial impacts of metamorphic remobilization on the Cu mineralization in the Zhongtiao region.

7. Conclusions

(1) The Huping Cu deposit comprises three alteration/mineralization stages, i.e., stage I veinlet–disseminated sulfides, stage II quartz–-sulfide veins and stage III calcite (–quartz) veins.
(2) The stage I mineralization has an albite + chlorite + biotite + epidote gangue mineral assemblage, and has deformed chalcopyrite with $\delta^{34}S$ values similar to the chlorite-amphibole schist wall rocks. This mineralization was likely resulted from mechanical Cu remobilization by solid-state ductile transfer under lower greenschist facies metamorphism.
(3) Chalcopyrite in the stage II mineralization was likely precipitated from metamorphic fluids (avg. $\delta^{18}O = 4.6‰$ and $\delta D = -56.6‰$) and has higher $\delta^{34}S$ values (avg. 8.0‰). The sulfur isotope signature was likely influenced by the incorporation of extra sulfur during the fluid migration. The stage II mineralization was likely related to metamorphic-hydrothermal Cu remobilization and precipitation via metamorphic-fluid immiscibility.
(4) The stage III quartz-calcite vein alteration (avg. $\delta^{18}O = 0.09‰$; $\delta^{13}C = -0.88‰$) may reflect meteoric fluid incursion into the waning metamorphic-hydrothermal system.
(5) Metamorphic-hydrothermal Cu remobilization may have had crucial impacts on the Cu mineralization in the Zhongtiao region.

Acknowledgements

This study was supported by the National Natural Science Foundation of China (No. 41672051) and Natural Science Foundation of Guangdong Province (No. 2016A030310115). We thank the Zhongtiaoshan Non-Ferrous Metals Group Co. Ltd. for its help in the fieldwork, Dr. Xi Liu for assisting the C–O isotope measurements and Dr. Changming Xing for the EPMA analysis. This is contribution No. IS-2572 from GIGCAS. The paper has benefited from constructive suggestions by the associate editor and two anonymous reviewers.

References

Bakker, R.J., 2012. Package FLUIDS. Part 4: thermodynamic modelling and purely empirical equations for H_2O-NaCl-KCl solutions. Mineral. Petrol. 105, 1–29.
Bakker, R.J., Diamond, L.W., 2000. Determination of the composition and molar volume of H_2O-CO_2 fluid inclusions by microthermometry. Geochim. Cosmochim. Acta 64, 1753–1764.
BGMR, 1965. Geologic map of Henan Province Sheet I-49-IV (Houma), I-49-V (Jincheng), I-49-X (Sanmenxia), and I-49-XI (Luoyang) scale 1:200,000.
Bickle, M.J., McKenzie, D., 1987. The transport of heat and matter by fluids during metamorphism. Contrib. Miner. Petrol. 95, 384–392.
Bodnar, R.J., 1993. Revised equation and table for determining the freezing-point depression of H_2O-NaCl solutions. Geochim. Cosmochim. Acta 57, 683–684.
Brown, P., 1998. Fluid inclusion modelling for hydrothermal systems. Rev. Econ. Geol. 10, 151–171.
Cartwright, I., Oliver, N., 2000. Metamorphic fluids and their relationship to the formation of metamorphosed and metamorphogenic ore deposits. Rev. Econ. Geol. 11, 81–96.
Cathelineau, M., 1988. Cation site occupancy in chlorites and illites as a function of temperature. Clay Miner. 23, 471–485.
Chen, H.Y., Chen, Y.J., Baker, M.J., 2012. Evolution of ore-forming fluids in the Sawayaerdun gold deposit in the Southwestern Chinese Tianshan metallogenic belt, Northwest China. J. Asian Earth Sci. 49, 131–144.
Chen, W.M., Li, S.P., 1998. Rhenium-osmium isotopic ages of sulfides from the Tongkuangyu porphyry copper deposit in the Zhongtiao mountain. Miner. Depos. 17, 224–228 (in Chinese with English abstract).
Chen, Y.J., Pirajno, F., Sui, Y.H., 2004. Isotope geochemistry of the Tieluping silver-lead deposit, Henan, China: a case study of orogenic silver-dominated deposits and related tectonic setting. Miner. Depos. 39, 560–575.
Chi, G.X., Savard, M.M., 1997. Sources of basinal and Mississippi Valley-type mineralizing brines: mixing of evaporated seawater and halite-dissolution brine. Chem. Geol. 143, 121–125.
Chinnasamy, S.S., Mishra, B., 2013. Greenstone metamorphism, hydrothermal alteration, and gold mineralization in the genetic context of the granodiorite-hosted gold deposit at Jonnagiri, eastern Dharwar Craton. Econ. Geol. 108, 1015–1036.
Clayton, R.N., Mayeda, T.K., Oneil, J.R., 1972. Oxygen isotope exchange between quartz and water. J. Geophys. Res. 77, 3057–3067.
Connolly, J.A.D., Thompson, A.B., 1989. Fluid and enthalpy production during regional metamorphism. Contrib. Miner. Petrol. 102, 347–366.
Deng, W.F., Wei, G.J., Xie, L.H., Yu, K.F., 2013. Environmental controls on coral skeletal delta C-13 in the northern South China Sea. J. Geophys. Res.-Biogeosci. 118, 1359–1368.
Diamond, L.W., 1992. Stability of CO_2 clathrate hydrate + CO_2 liquid + CO_2 vapor + aqueous KCl-NaCl solutions: experimental determination and application to salinity estimates of fluid inclusions. Geochim. Cosmochim. Acta 56, 273–280.
Ding, T., Valkiers, S., Kipphardt, H., De Bievre, P., Taylor, P.D.P., Gonfiantini, R., et al., 2001. Calibrated sulfur isotope abundance ratios of three IAEA sulfur isotope reference materials and V-CDT with a reassessment of the atomic weight of sulfur. Geochim. Cosmochim. Acta 65, 2433–2437.
Driesner, T., 2007. The system H_2O–NaCl. Part II: Correlations for molar volume, enthalpy, and isobaric heat capacity from 0 to 1000 °C, 1 to 5000 bar, and 0 to 1 X_{NaCl}. Geochim. Cosmochim. Acta 71, 4902–4919.
Elmer, F.L., Powell, R., White, R.W., Phillips, G.N., 2007. Timing of gold mineralization relative to the peak of metamorphism at Bronzewing, Western Australia. Econ. Geol. 102, 379–392.
Faure, 1986. Principles of Isotope Geology. John Wiley & Sons, New York.
Feng, Z.P., Wang, Y.H., 2008. Strata division in Songjiashan subgroup of Late Archean Jiangxian Group in Zhongtiaoshan area. Shanxi Metallurgy 6, 20–22 (in Chinese with English abstract).
Ferry, J.M., Dipple, G.M., 1991. Fluid flow, mineral reactions, and metasomatism. Geology 19, 211–214.
Goldfarb, R.J., Groves, D.I., 2015. Orogenic gold: Common or evolving fluid and metal sources through time. Lithos 233, 2–26.
Hall, D.L., Sterner, S.M., Bodnar, R.J., 1988. Freezing point depression of NaCl-KCl-H_2O solutions. Econ. Geol. 83, 197–202.
Han, W.D., He, Q., Liu, J.H., 2005. Study of the prospecting ore of Luojiahe copper ore in Zhongtiaoshan. Shanxi Metallurgy 13–14, 43 (in Chinese with English abstract).
He, Y.H., Zhao, G.C., Sun, M., Wilde, S.A., 2008. Geochemistry, isotope systematics and petrogenesis of the volcanic rocks in the Zhongtiao Mountain: an alternative interpretation for the evolution of the southern margin of the North China Craton. Lithos 102, 158–178.
Hemley, J., Cygan, G., Fein, J., Robinson, G., d'Angelo, W., 1992. Hydrothermal ore-forming processes in the light of studies in rock-buffered systems: I, iron-copper-zinc-lead sulfide solubility relations. Econ. Geol. 87, 1–22.
Hey, M.H., 1954. A new review of the chlorites. Mineral. Mag. 30, 277–292.
Hoefs, J., 2009. Variations of stable isotope ratios in nature. In: Hoefs, J. (Ed.), Stable Isotope Geochemistry. Springer-Verlag, Berlin, pp. 93–227.
Hu, W.X., Sun, D.H., 1987. Mineralization and evolution of the early Proterozoic copper deposits in the Zhongtiao Mountains. Acta Geol. Sin. 61, 61–76.
Jiang, Y., Zhao, Y., Niu, H., 2016. Paleoproterozoic copper system in the Zhongtiaoshan region, southern margin of the North China Craton: Ore geology, fluid inclusion, and isotopic investigation. In: Zhai, M.G., Zhao, Y., Zhao, T.P. (Eds.), Main Tectonic Events and Metallogeny of the North China Craton. Springer-Verlag, Berlin, pp. 229–250.
Jiang, Y.H., Niu, H.C., Bao, Z.W., Li, N.B., Shan, Q., Yang, W.B., 2014a. Fluid evolution of the Tongkuangyu porphyry copper deposit in the Zhongtiaoshan region: evidence from fluid inclusions. Ore Geol. Rev. 63, 498–509.
Jiang, Y.H., Niu, H.C., Bao, Z.W., Li, N.B., Shan, Q., Yang, W.B., Yan, S., 2014b. Fluid evolution of the Paleoproterozoic Hujiayu copper deposit in the Zhongtiaoshan region: evidence from fluid inclusions and carbon-oxygen isotopes. Precambr. Res. 255, 734–747.
Jiang, Y.H., Niu, H.C., Zhao, Y., Bao, Z.W., Li, N.B., Shan, Q., 2017. Fluid inclusion and stable isotopic constraints on fluid sources and evolution of the Luojiahe Cu deposit in the southern margin of the North China Craton. Ore Geol. Rev. 80, 214–228.
Klemm, L.M., Pettke, T., Heinbicth, C.A., Campos, E., 2007. Hydrothermal evolution of the El Teniente deposit, Chile: porphyry Cu-Mo ore deposition from low-salinity magmatic fluids. Econ. Geol. 102, 1021–1045.
Landtwing, M.R., Pettke, T., Halter, W.E., Heinrich, C.A., Redmond, P.B., Einaudi, M.T.,

Kunze, K., 2005. Copper deposition during quartz dissolution by cooling magmatic-hydrothermal fluids: The Bingham porphyry. Earth Planet. Sci. Lett. 235, 229–243.
Liu, C.H., Zhao, G.C., Sun, M., Zhang, J., Yin, C.Q., 2012. U-Pb geochronology and Hf isotope geochemistry of detrital zircons from the Zhongtiao Complex: constraints on the tectonic evolution of the Trans-North China Orogen. Precambr. Res. 222, 159–172.
Liu, D.Y., Nutman, A.P., Compston, W., Wu, J.S., Shen, Q.H., 1992. Remnants of greater than or equal to 3800 Ma crust in the Chinese part of the Sino-Korean Craton. Geology 20, 339–342.
Liu, S.W., Zhao, G.C., Wilde, S.A., Shu, G.M., Sun, M., Li, Q.G., Tian, W., Zhang, J., 2006. Th-U-Pb monazite geochronology of the Lüliang and Wutai Complexes: constraints on the tectonothermal evolution of the Trans-North China Orogen. Precambr. Res. 148, 205–224.
Liu, X., Fan, H.R., Qiu, Z.J., Yang, K.F., Hu, F.F., Guo, S.L., et al., 2015. Formation ages of the Jiangxian and Zhongtiao groups in the Zhongtiao Mountain region, North China Craton: Insights from SIMS U-Pb dating on zircons of intercalated plagioclase amphibolites. Acta Petrol. Sin. 31, 1564–1572 (in Chinese with English abstract).
Liu, X., Fan, H.R., Santosh, M., Yang, K.F., Qiu, Z.J., Hu, F.F., Wen, B.J., 2016. Geological and geochronological constraints on the genesis of the giant Tongkuangyu Cu deposit (Paleoproterozoic), North China Craton. Int. Geol. Rev. 58, 155–170.
Marshall, B., Gilligan, L.B., 1987. An introduction to remobilization: Information from ore-body geometry and experimental considerations. Ore Geol. Rev. 2, 87–131.
Marshall, B., Gilligan, L.B., 1993. Remobilization, syn-tectonic processes and massive sulfide deposits. Ore Geol. Rev. 8, 39–64.
Marshall, B., Vokes, F., Larocque, A., 2000. Regional metamorphic remobilization: upgrading and formation of ore deposits. Rev. Econ. Geol. 11, 19–38.
Mishra, B., Pal, N., 2008. Metamorphism, fluid flux, and fluid evolution relative to gold mineralization in the Hutti-Maski greenstone belt, eastern Dharwar craton, India. Econ. Geol. 103, 801–827.
Mishra, B., Pal, N., Sarbadhikari, A.B., 2005. Fluid inclusion characteristics of the Uti gold deposit, Hutti-Maski greenstone belt, southern India. Ore Geol. Rev. 26, 1–16.
Mishra, B., Pruseth, K.L., Hazarika, P., Chinnasamy, S.S., 2017. Nature and source of the ore-forming fluids associated with orogenic gold deposits in the Dharwar Craton. Geosci. Front (10.1016/j.gsf.2017.09.005).
Mookherjee, A., 1970a. Dykes, sulfide deposits, and regional metamorphism: criteria for determining their time relationship. Miner. Depos. 5, 120–144.
Mookherjee, A., 1970b. Metamorphic and metamorphosed sulfide deposits. Econ. Geol. 65, 886–889.
Mountain, B., Seward, T., 2003. Hydrosulfide/sulfide complexes of copper (I): experimental confirmation of the stoichiometry and stability of Cu $(HS)^{2-}$ to elevated temperatures. Geochim. Cosmochim. Acta 67, 3005–3014.
Mukwakwami, J., Lafrance, B., Lesher, C.M., Tinkham, D.K., Rayner, N.M., Ames, D.E., 2014a. Geochemistry of deformed and hydrothermally mobilized magmatic Ni-Cu-PGE ores at the Garson Mine, Sudbury. Miner. Depos. 49, 175–198.
Mukwakwami, J., Lesher, C.M., Lafrance, B., 2014b. Geochemistry of deformed and hydrothermally mobilized magmatic Ni-Cu-PGE ores at the Garson mine, Sudbury. Econ. Geol. 109, 367–386.
O'Neil, J.R., Clayton, R.N., Mayeda, T.K., 1969. Oxygen isotope fractionation in divalent metal carbonates. J. Chem. Phys. 51, 5547–5558.
Ohmoto, H., Goldhaber, M.B., 1997. Sulfur and carbon isotopes, geochemistry of hydrothermal ore deposits. New York, John Wiley & Sons 517–611.
Oliver, N.H.S., 1996. Review and classification of structural controls on fluid flow during regional metamorphism. J. Metamorph. Geol. 14, 477–492.
Peng, H.J., Mao, J.W., Hou, L., Shu, Q.H., Zhang, C.Q., Liu, H., Zhou, Y.M., 2016. Stable isotope and fluid inclusion constraints on the source and evolution of ore fluids in the Hongniu-Hongshan Cu skarn deposit, Yunnan Province, China. Econ. Geol. 111, 1369–1396.
Pirajno, F., 1992. Hydrothermal Mineral Deposits: Principles and Fundamental Concepts for the Exploration Geologist. Springer-Verlag, Berlin, pp. 42–100.
Pohl, W.L., 2011. Economic Geology: Principles and Practice. John Wiley & Sons, New York.
Qiu, Z.G., Fan, H.R., Liu, X., Wen, B.J., Hu, F.F., Yang, K.F., Guo, S.L., Zhao, F.C., 2015a. Fluid inclusion and Carbon-Oxygen isotope studies of the Hujiayu Cu deposit, Zhongtiao Mountains, China: implications for syn-metamorphic copper remobilization. Acta Geol. Sin. 89, 726–745.
Qiu, Z.J., Fan, H.R., Liu, X., Yang, K.F., Hu, F.F., Cai, Y.C., 2017a. Metamorphic PTt evolution of Paleoproterozoic schist-hosted Cu deposits in the Zhongtiao Mountains, North China Craton: retrograde ore formation during sluggish exhumation. Precambr. Res. 300, 59–77.
Qiu, K.F., Song, K.R., Song, Y.H., 2015b. Magmatic-hydrothermal fluid evolution of the Wenquan porphyry molybdenum deposit in the north margin of the Western Qinling, China. Acta Petrol. Sin. 31, 3391–3404 (in Chinese with English abstract).
Qiu, K.F., Taylor, R.D., Song, Y.H., Yu, H.C., Song, K.R., Li, N., 2016a. Geologic and geochemical insights into the formation of the Taiyangshan porphyry copper-molybdenum deposit, Western Qinling Orogenic Belt, China. Gondwana Res. 35, 40–58.
Qiu, K.F., Deng, J., Taylor, R.D., Song, K.R., Song, Y.H., Li, Q.Z., et al., 2016b. Paleozoic magmatism and porphyry Cu-mineralization in an evolving tectonic setting in the North Qilian Orogenic Belt, NW China. J. Asian Earth Sci. 122, 20–40.
Qiu, K.F., Marsh, E., Yu, H.C., Pfaff, K., Gulbransen, C., Gou, Z.Y., et al., 2017b. Fluid and metal sources of the Wenquan porphyry molybdenum deposit, Western Qinling, NW China. Ore Geol. Rev. 86, 459–473.
Ramboz, C., Pichavant, M., Weisbrod, A., 1982. Fluid immiscibility in natural processes: use and misuse of fluid inclusion data: II. Interpretation of fluid inclusion data in terms of immiscibility. Chem. Geol. 37, 29–48.
Robb, L., 2013. Introduction to Ore-Forming Processes. John Wiley & Sons, New York.
Saravanan, C.S., Mishra, B., Jairam, M.S., 2009. P-T conditions of mineralization in the Jonnagiri granitoid-hosted gold deposit, eastern Dharwar Craton, southern India: constraints from fluid inclusions and chlorite thermometry. Ore Geol. Rev. 36, 333–349.
Spear, F.S., 1995. Metamorphic Phase Equilibria and Pressure-Temperature-Time Paths. Mineralogical Society of America Washington, Washington.
Stowell, H.H., Lesher, C.M., Green, N.L., Sha, P., Guthrie, G.M., Sinha, A.K., 1996. Metamorphism and gold mineralization in the Blue Ridge, southernmost Appalachians. Econ. Geol. 91, 1115–1144.
Sun, D.Z., Hu, W.X., 1993. Precambrian geochronology, chronotectonic framework and model of chronocrustal structure of the Zhongtiao Mountains. Geological Publishing House, Beijing (in Chinese).
Sun, D.Z., Hu, W.X., Tang, M., Zhao, F.Q., Condie, K.C., 1990. Origin of Late Archean and Early Proterozoic rocks and associated mineral deposits from the Zhongtiao Mountains, East-Central China. Precambr. Res. 47, 287–306.
Sun, D.Z., Li, H.M., Lin, Y.X., Zhou, H.F., Zhao, F.Q., Tang, M., 1992. Precambrian geochronology, chronotectonic framework and model of chronocrustal structure of the Zhongtiao Mountains. Acta Geol. Sin. 5, 23–37.
Sun, J.Y., Ji, S.K., Zhen, Y.Q., 1995. The Copper Deposits in the Zhongtiao Rift. Geological Publishing House, Beijing (in Chinese with English abstract).
Sun, Y., Yu, Z.P., 1988. Geochemistry of Archean Shushui Complex. Geochemica 4, 319–325 (in Chinese with English abstract).
Taylor, H., 1974. The application of oxygen and hydrogen isotope studies to problems of hydrothermal alteration and ore deposition. Econ. Geol. 69, 843–883.
Tomkins, A.G., 2007. Three mechanisms of ore re-mobilization during amphibolite facies metamorphism at the Montauban Zn-Pb-Au-Ag deposit. Miner. Deposita 42, 627–637.
Tomkins, A.G., 2010. Windows of metamorphic sulfur liberation in the crust: Implications for gold deposit genesis. Geochim. Cosmochim. Acta 74, 3246–3259.
Trap, P., Faure, M., Lin, W., Meffre, S., 2009. The Lüliang Massif: a key area for the understanding of the Paleoproterozoic Trans-North China Belt, North China Craton. Geological Society, London, Special Publications 323, 99–125.
Turlin, F., Eglinger, A., Vanderhaeghe, O., André-Mayer, A.-S., Poujol, M., Mercadier, J., Bartlett, R., 2016. Synmetamorphic Cu remobilization during the Pan-African orogeny: Microstructural, petrological and geochronological data on the kyanite-mica schists hosting the Cu (–U) Lumwana deposit in the Western Zambian Copperbelt of the Lufilian belt. Ore Geol. Rev. 75, 52–75.
Wan, Y., Wilde, S.A., Liu, D., Yang, C., Song, B., Yin, X., 2006. Further evidence for ~1.85 Ga metamorphism in the Central Zone of the North China Craton: SHRIMP U-Pb dating of zircon from metamorphic rocks in the Lushan area, Henan Province. Gondwana Res. 9, 189–197.
Wang, G.G., Ni, P., Wang, R.C., Zhao, K.D., Chen, H., Ding, J.Y., Zhao, C., Cai, Y.T., 2013. Geological, fluid inclusion and isotopic studies of the Yinshan Cu-Au-Pb-Zn-Ag deposit, South China: Implications for ore genesis and exploration. J. Asian Earth Sci. 74, 343–360.
Wang, H.K., 2014. Genesis of copper deposits in Tongshan, Yuanqu, Shanxi Province. Huabei Land and Resources 91–92, 101 (in Chinese).
Wang, P., Pan, Z., Weng, L., 1982. Systematic Mineralogy. Geology Publishing House, Beijing (in Chinese).
Weatherley, D.K., Henley, R.W., 2013. Flash vaporization during earthquakes evidenced by gold deposits. Nat. Geosci. 6, 294–298.
WGCGZM, 1978. Copper geology of the Zhongtiao Mountains. Geological Publishing House, Beijing.
Williams-Jones, A., Samson, I., Ault, K., Gagnon, J., Fryer, B., 2010. The genesis of distal zinc skarns: Evidence from the Mochito deposit, Honduras. Econ. Geol. 105, 1411–1440.
Xiao, Z., Gammons, C.H., Williams-Jones, A.E., 1998. Experimental study of copper (I) chloride complexing in hydrothermal solutions at 40 to 300 °C and saturated water vapor pressure. Geochim. Cosmochim. Acta 62, 2949–2964.
Xing, C.M., Wang, C.Y., 2017. Cathodoluminescence images and trace element compositions of fluorapatite from the Hongge layered intrusion in SW China: a record of prolonged crystallization and overprinted fluid metasomatism. Am. Mineral. 102, 1390–1401.
Xu, Q.L., 2010. Study on the geological characteristics and ore genesis of Tongkuangyu copper deposit in the Zhongtiaoshan Mountains, Shanxi Province. (Master's thesis) Jilin University, Changchun (in Chinese with English abstract).
Zhai, M., 2010. Tectonic evolution and metallogenesis of North China Craton. Miner. Depos. 29, 24–36 (in Chinese with English abstract).
Zhai, M.G., 2013. Secular changes of metallogenic systems link with continental evolving of the North China Craton. Acta Petrol. Sin. 29, 1759–1773 (in Chinese with English abstract).
Zhai, M.G., Santosh, M., 2011. The early Precambrian odyssey of the North China Craton: a synoptic overview. Gondwana Res. 20, 6–25.
Zhai, M.G., Santosh, M., 2013. Metallogeny of the North China Craton: link with secular changes in the evolving Earth. Gondwana Res. 24, 275–297.
Zhang, H., 2012. Metallogenesis of Paleoproterozoic copper deposits in the Northern Zhongtiaoshan Mountains, Shanxi Province. (PhD thesis) Jilin University, Changchun (in Chinese with English abstract).
Zhang, R.Y., 2015. The composition and evolution of the Sushui complex in the Zhongtiao Mountains, the south of North China Craton. (PhD thesis) Northwest University, Xi'an (in Chinese with English abstract).
Zhang, Y.J., Sun, F.Y., Li, B.L., Huo, L., Ma, F., 2014. Ore textures and remobilization mechanisms of the Hongtoushan copper-zinc deposit, Liaoning, China. Ore Geol. Rev. 57, 78–86.
Zhao, C., Ni, P., Wang, G.G., Ding, J.Y., Chen, H., Zhao, K.D., Cai, Y.T., Xu, Y.F., 2013. Geology, fluid inclusion, and isotope constraints on ore genesis of the Neoproterozoic Jinshan orogenic gold deposit, South China. Geofluids 13, 506–527.

Zhao, G.C., Wilde, S.A., Sun, M., Li, S.Z., Li, X.P., Zhang, J., 2008. SHRIMP U-Pb zircon ages of granitoid rocks in the Lüliang Complex: Implications for the accretion and evolution of the Trans-North China Orogen. Precambr. Res. 160, 213–226.
Zhao, G.C., Zhai, M.G., 2013. Lithotectonic elements of Precambrian basement in the North China Craton: Review and tectonic implications. Gondwana Res. 23, 1207–1240.
Zhao, T.P., Xu, Y.H., Zhai, M.G., 2007. Petrogenesis and tectonic setting of the Paleoproterozoic Xiong'er Group in the southern part of the North China Craton: a review. Geol. J. China Univers. 2, 191–206 (in Chinese with English abstract).
Zhu, Z.Y., Cook, N.J., Yang, T., Ciobanu, C.L., Zhao, K.D., Jiang, S.Y., 2016. Mapping of sulfur isotopes and trace elements in sulfides by LA-(MC)-ICP-MS: potential analytical problems, improvements and implications. Minerals 6, 110.
Zhu, Z.Y., Jiang, S.Y., Ciobanu, C.L., Yang, T., Cook, N.J., 2017. Sulfur isotope fractionation in pyrite during laser ablation: Implications for laser ablation multiple collector inductively coupled plasma mass spectrometry mapping. Chem. Geol. 450, 223–234.